CHAPTER

7

Gravity Waves

OUTLINE

CHAPTER OBJECTIVES

- To develop the equations and boundary conditions for surface, interface, and internal waves.
- To derive linear gravity-capillary wave propagation speed(s), pressure fluctuations, dispersion, particle motion, and energy flux for surface waves on a liquid layer of arbitrary but constant depth.
- To describe and highlight wave refraction and nonlinear gravity wave results in shallow and deep water.
- To determine linear density-interface wave characteristics with and without an additional free surface.
- To present the characteristics of gravity waves on a density gradient with constant buoyancy frequency.

7.1. INTRODUCTION

There are three types of waves commonly considered in the study of fluid mechanics: interface waves, internal waves, and compression and expansion waves. In all cases, the waves are traveling fluid oscillations, impulses, or pressure changes sustained by the interplay of fluid inertia and a restoring force or a pressure imbalance. For interface waves the restoring forces are gravity and surface tension. For internal waves, the restoring force is gravity. For expansion and compression waves, the restoring force comes directly from the compressibility of the fluid. The basic elements of linear and nonlinear compression and expansion waves are presented in Chapter 15, which covers compressible fluid dynamics. This chapter covers interface and internal waves with an emphasis on gravity as the restoring force. The approach and results from the prior chapter will be exploited here since the wave physics and wave phenomena presented in this chapter primarily involve irrotational flow.

Perhaps the simplest and most readily observed fluid waves are those that form and travel on the density discontinuity provided by an air-water interface. Such s*urface gravity-capillary waves*, sometimes simply called *water waves*, involve fluid particle motions parallel and perpendicular to the direction of wave propagation. Thus, the waves are neither longitudinal nor transverse. When generalized to internal waves that propagate in a fluid medium having a continuous density gradient, the situation may be even more complicated. This chapter presents some basic features of wave motion and illustrates them with water waves because water wave phenomena are readily observed and this aids comprehension. Throughout this chapter, the wave frequency will be assumed much higher than the Coriolis frequency so the wave motion is unaffected by the earth's rotation. Waves affected by planetary rotation are considered in Chapter 13. And, unless specified otherwise, wave amplitudes are assumed small enough so that the governing equations and boundary conditions are linear.

For such linear waves, Fourier superposition of sinusoidal waves allows arbitrary waveforms to be constructed and sinusoidal waveforms arise naturally from the linearized equations for water waves (see Exercise 7.3). Consequently, a simple sinusoidal traveling wave of the form

$$\eta(x,t) = a\cos\left[\frac{2\pi}{\lambda}(x-ct)\right] \tag{7.1}$$

is a foundational element for what follows. In Cartesian coordinates with x horizontal and z vertical, $z = \eta(x,t)$ specifies the *waveform* or surface shape where a is the wave *amplitude*, λ is the *wavelength*, c is the *phase speed*, and $2\pi(x - ct)/\lambda$ is the *phase*. In addition, the spatial frequency $k \equiv 2\pi/\lambda$, with units of rad./m, is known as the *wave number*. If (7.1) describes the vertical deflection of an air-water interface, then the height of wave crests is $+a$ and the depth of the wave troughs is $-a$ compared to the undisturbed water-surface location $y = 0$. At any instant in time, the distance between successive wave crests is λ. At any fixed x-location, the time between passage of successive wave crests is the *period*, $T = 2\pi/kc = \lambda/c$. Thus, the wave's *cyclic frequency* is $\nu = 1/T$ with units of Hz, and its *radian frequency* is $\omega = 2\pi\nu$ with units of rad./s. In terms of k and ω, (7.1) can be written:

$$\eta(x,t) = a\cos[kx - \omega t]. \tag{7.2}$$

The wave propagation speed is readily deduced from (7.1) or (7.2) by determining the travel speed of wave crests. This means setting the phase in (7.1) or (7.2) so that the cosine function is unity and $\eta = +a$. This occurs when the phase is $2n\pi$ where n is an integer,

$$\frac{2\pi}{\lambda}(x_{crest} - ct) = 2n\pi = kx_{crest} - \omega t, \tag{7.3}$$

and x_{crest} is the time-dependent location where $\eta = +a$. Solving for the crest location produces:

$$x_{crest} = (\omega/k)t + 2n\pi/k.$$

Therefore, in a time increment Δt, a wave crest moves a distance $\Delta x_{crest} = (\omega/k)\Delta t$. Thus,

$$c = \omega/k = \lambda\nu \tag{7.4}$$

is known as the phase speed because it specifies the travel speed of constant-phase wave features, like wave crests or troughs.

Although instructive, (7.1) and (7.2) are limited to propagation in the positive x direction only. In general, waves may propagate in any direction. A useful three-dimensional generalization of (7.2) is:

$$\eta = a\cos(kx + ly + mz - \omega t) = a\cos(\mathbf{K}\cdot\mathbf{x} - \omega t), \tag{7.5}$$

where $\mathbf{K} = (k, l, m)$ is a vector, called the *wave number vector*, whose magnitude is given by

$$K^2 = k^2 + l^2 + m^2. \tag{7.6}$$

The wavelength derived from (7.5) is

$$\lambda = 2\pi/K, \tag{7.7}$$

which is illustrated in Figure 7.1 in two dimensions. The magnitude of the phase velocity is $c = \omega/K$, and the direction of propagation is parallel to $\mathbf{K}$, so the phase velocity vector is:

$$\mathbf{c} = (\omega/K)\mathbf{e}_K, \tag{7.8}$$

where $\mathbf{e}_K = \mathbf{K}/K$.

From Figure 7.1, it is also clear that $c_x = \omega/k$, $c_y = \omega/l$, and $c_z = \omega/m$ are each larger than the resultant $c = \omega/K$, because k, l, and m are individually smaller than K when all three are nonzero, as required by (7.6). Thus, c_x, c_y, and c_z are not vector components of the phase velocity in the usual sense, but they do reflect the fact that constant-phase surfaces appear to travel faster along directions not coinciding with the direction of propagation, the x and y directions in Figure 7.1 for example. Any of the three axis-specific phase speeds is sometimes called the *trace velocity* along its associated axis.

If sinusoidal fluid waves exist in a fluid moving with uniform speed $\mathbf{U}$, then the observed phase speed is $\mathbf{c}_0 = \mathbf{c} + \mathbf{U}$. Forming a dot product of $\mathbf{c}_0$ with $\mathbf{K}$, and using (7.8), produces

$$\omega_0 = \omega + \mathbf{U}\cdot\mathbf{K}, \tag{7.9}$$

where ω_0 is the *observed frequency* at a fixed point, and ω is the *intrinsic frequency* measured by an observer moving with the flow. It is apparent that the frequency of

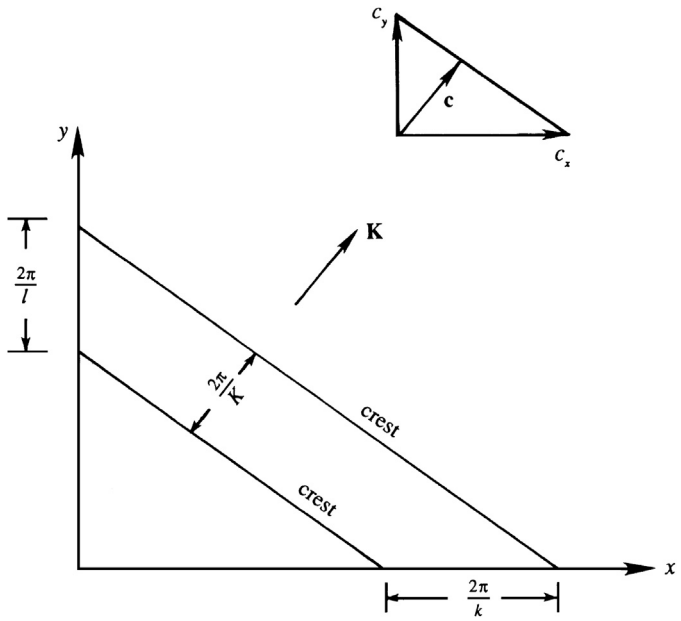

FIGURE 7.1 Wave crests propagating in the x-y plane. The crest spacing along the coordinate axes is larger than the wavelength $\lambda = 2\pi/K$. The inset shows how the trace velocities c_x and c_y are combined to give the phase velocity vector **c**.

a wave is *Doppler shifted* by an amount $\mathbf{U}\cdot\mathbf{K}$ in nonzero flow. Equation (7.9) may be understood by considering a situation in which the intrinsic frequency ω is zero, but the flow pattern has a periodicity in the x direction of wavelength $2\pi/k$. If this sinusoidal pattern is translated in the x direction at speed U, then the observed frequency at a fixed point is $\omega_0 = Uk$. The effects of uniform flow on frequency will not be considered further, and all frequencies in the remainder of this chapter should be interpreted as intrinsic frequencies.

7.2. LINEAR LIQUID-SURFACE GRAVITY WAVES

Starting from the equations for ideal flow, this section develops the properties of small-slope, small-amplitude gravity waves on the free surface of a constant-density liquid layer of uniform depth H, which may be large or small compared to the wavelength λ. The limitation to waves with small slopes and amplitudes implies $a/\lambda \ll 1$ and $a/H \ll 1$, respectively. These two conditions allow the problem to be linearized. In this first assessment of wave motion, surface tension is neglected for simplicity; in water its effect is limited to wavelengths less than 5 to 10 centimeters, as discussed in Section 7.3. In addition, the air above the liquid is ignored, and the liquid's motion is presumed to be irrotational and entirely caused by the surface waves.

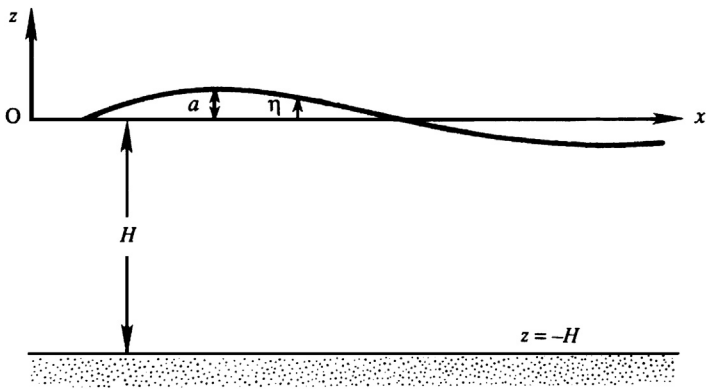

FIGURE 7.2 Geometry for determining the properties of linear gravity waves on the surface of a liquid layer of depth H. Gravity points downward along the z-axis. The undisturbed liquid surface location is $z = 0$ so the bottom is located at $z = -H$. The surface's vertical deflection or waveform is $\eta(x,t)$. When η is sinusoidal, its peak deflection from $z = 0$ is the sinusoid's amplitude a.

To get started, choose the x-axis in the direction of wave propagation with the z-axis vertical so that the motion is two dimensional in the x-z plane (Figure 7.2). Let $\eta(x,t)$ denote the vertical liquid-surface displacement from its undisturbed location $z = 0$. Because the liquid's motion is irrotational, a velocity potential $\phi(x, z, t)$ can be defined such that

$$u = \partial\phi/\partial x, \quad \text{and} \quad w = \partial\phi/\partial z, \tag{7.10}$$

so the incompressible continuity equation $\partial u/\partial x + \partial w/\partial z = 0$ implies

$$\partial^2\phi/\partial x^2 + \partial^2\phi/\partial z^2 = 0. \tag{7.11}$$

There are three boundary conditions. The condition at the bottom of the liquid layer is zero normal velocity, that is,

$$w = \partial\phi/\partial z = 0 \quad on \quad z = -H. \tag{7.12}$$

At the free surface, a *kinematic boundary condition* is applied that requires the fluid-particle velocity normal to the surface, $\mathbf{u}\cdot\mathbf{n}$, and on the surface be the same as the velocity of the surface $\mathbf{U}_s$ normal to itself:

$$(\mathbf{n}\cdot\mathbf{u})_{z=\eta} = \mathbf{n}\cdot\mathbf{U}_s, \tag{7.13}$$

where $\mathbf{n}$ is the surface normal. This ensures that the liquid elements that define the interface do not become separated from the interface while still allowing these interface elements to move along the interface.

For the current situation, the equation for the surface may be written $f(x, z, t) = z - \eta(x, t) = 0$, so the surface normal $\mathbf{n}$, which points upward out of the liquid will be:

$$\mathbf{n} = \nabla f/|\nabla f| = (-(\partial\eta/\partial x)\mathbf{e}_x + \mathbf{e}_z)/\sqrt{(\partial\eta/\partial x)^2 + 1}. \tag{7.14}$$

The velocity of the surface $\mathbf{U}_s$ at any location x can be considered purely vertical:

$$\mathbf{U}_s = (\partial\eta/\partial t)\mathbf{e}_z. \tag{7.15}$$

Thus, (7.13) multiplied by $|\nabla f|$ implies $(\nabla f \cdot \mathbf{u})_{z=\eta} = \nabla f \cdot \mathbf{U_s}$, which can be evaluated using (7.14) and $\mathbf{u} = u\mathbf{e}_x + w\mathbf{e}_z$ to find:

$$\left(-u\frac{\partial \eta}{\partial x} + w\right)_{z=\eta} = \frac{\partial \eta}{\partial t}, \quad \text{or} \quad \left(\frac{\partial \phi}{\partial z}\right)_{z=\eta} = \frac{\partial \eta}{\partial t} + \frac{\partial \eta}{\partial x}\left(\frac{\partial \phi}{\partial x}\right)_{z=\eta}, \tag{7.16}$$

where (7.10) has been used for the fluid velocity components to achieve the second form of (7.16). For small-slope waves, the final term in (7.16) is small compared to the other two, so the kinematic boundary condition can be approximated:

$$\left(\frac{\partial \phi}{\partial z}\right)_{z=\eta} \cong \frac{\partial \eta}{\partial t}. \tag{7.17}$$

For consistency, the left side of (7.17) must also be approximated for small wave slopes, and this is readily accomplished via a Taylor series expansion around $z = 0$:

$$\left(\frac{\partial \phi}{\partial z}\right)_{z=\eta} = \left(\frac{\partial \phi}{\partial z}\right)_{z=0} + \eta\left(\frac{\partial^2 \phi}{\partial z^2}\right)_{z=0} + \ldots \cong \frac{\partial \eta}{\partial t}.$$

Thus, when a/λ is small enough, the simplest version of (7.13) is

$$\left(\frac{\partial \phi}{\partial z}\right)_{z=0} \cong \frac{\partial \eta}{\partial t}. \tag{7.18}$$

These simplifications of the kinematic boundary are justified when $ka = 2\pi a/\lambda \ll 1$ (see Exercise 7.2).

In addition to the kinematic condition at the surface, there is a *dynamic condition* that the pressure just below the liquid surface be equal to the ambient pressure, with surface tension neglected. Taking the ambient air pressure above the liquid to be a constant atmospheric pressure, the dynamic surface condition can be stated,

$$(p)_{z=\eta} = 0, \tag{7.19}$$

where p in (7.19) is the gauge pressure. Equation (7.19) follows from the boundary condition on $\boldsymbol{\tau} \cdot \mathbf{n}$, which is continuous across an interface as established in Section 4.10. Equation (7.19) and the neglect of any shear stresses on $z = \eta$ define a stress-free boundary. Thus, the water surface in this ideal case is commonly called a *free surface*. For consistency, this condition should also be simplified for small-slope waves by dropping the nonlinear term $|\nabla \phi|^2$ in the relevant Bernoulli equation (4.83):

$$\frac{\partial \phi}{\partial t} + \frac{p}{\rho} + gz \cong 0, \tag{7.20}$$

where the Bernoulli constant has been evaluated on the undisturbed liquid surface far from the surface wave. Evaluating (7.20) on $z = \eta$ and applying (7.19) produces:

$$\left(\frac{\partial \phi}{\partial t}\right)_{z=\eta} \cong \left(\frac{\partial \phi}{\partial t}\right)_{z=0} \cong -g\eta. \tag{7.21}$$

The first approximate equality follows because $(\partial\phi/\partial t)_{z=0}$ is the first term in a Taylor series expansion of $(\partial\phi/\partial t)_{z=\eta}$ in powers of η about $\eta = 0$. This approximation is consistent with (7.18).

Interestingly, even with the specification of the field equation (7.11) and the three boundary conditions, (7.12), (7.18), and (7.21), the overall linear surface-wave problem is not fully defined without initial conditions for the surface shape (Exercise 7.3). For simplicity, we chose $\eta(x,\ t=0)=a\cos(kx)$, since it is satisfied by the simple sinusoidal wave (7.2), which now becomes a foundational part of the solution. To produce a cosine dependence for η on the phase $(kx-\omega t)$ in (7.2), conditions (7.18) and (7.21) require ϕ to be a sine function of $(kx-\omega t)$. Consequently, a solution is sought for ϕ in the form

$$\phi(x,z,t)=f(z)\,\sin(kx-\omega(k)t), \tag{7.22}$$

where $f(z)$ and $\omega=\omega(k)$ are to be determined. Substitution of (7.22) into the Laplace equation (7.11) gives

$$d^2f/dz^2-k^2f=0,$$

which has the general solution $f(z)=Ae^{kz}+Be^{-kz}$, where A and B are constants. Thus, (7.22) implies

$$\phi=(Ae^{kz}+Be^{-kz})\,\sin(kx-\omega t). \tag{7.23}$$

The constants A and B can be determined by substituting (7.23) into (7.12):

$$k(Ae^{-kH}-Be^{+kH})\,\sin(kx-\omega t)=0 \text{ or } B=Ae^{-2kH}, \tag{7.24}$$

and by substituting (7.2) and (7.23) into (7.18),

$$k(A-B)\,\sin(kx-\omega t)=\omega a\sin(kx-\omega t) \text{ or } k(A-B)=\omega a. \tag{7.25}$$

Solving (7.24) and (7.25) for A and B produces:

$$A=\frac{a\omega}{k\left(1-e^{-2kH}\right)} \qquad B=\frac{a\omega\, e^{-2kH}}{k\left(1-e^{-2kH}\right)}.$$

The velocity potential (7.23) then becomes:

$$\phi=\frac{a\omega}{k}\frac{\cosh(k(z+H))}{\sinh(kH)}\sin(kx-\omega t), \tag{7.26}$$

from which the fluid velocity components are found as:

$$u=a\omega\frac{\cosh(k(z+H))}{\sinh(kH)}\cos(kx-\omega t), \text{ and } w=a\omega\frac{\sinh(k(z+H))}{\sinh(kH)}\sin(kx-\omega t). \tag{7.27}$$

This solution of the Laplace equation has been found using kinematic boundary conditions alone, and this is typical of irrotational constant-density flows where fluid pressure is determined through a Bernoulli equation after the velocity field has been found. Here the dynamic surface boundary condition (7.21) enforces $p=0$ on the liquid surface, and substitution of (7.2) and (7.26) into (7.21) produces:

$$\left(\frac{\partial\phi}{\partial t}\right)_{z=0}=-\frac{a\omega^2}{k}\frac{\cosh(kH)}{\sinh(kH)}\cos(kx-\omega t)\cong-g\eta=-ag\,\cos(kx-\omega t),$$

which simplifies to a relation between ω and k (or equivalently, between the wave period T and the wave length λ):

$$\omega = \sqrt{gk\tanh(kH)} \text{ or } T = \sqrt{\frac{2\pi\lambda}{g}\coth\left(\frac{2\pi H}{\lambda}\right)}. \tag{7.28}$$

The first part of (7.28) specifies how temporal and spatial frequencies of the surface waves are related, and it is known as a *dispersion relation*. The phase speed c of these surface waves is given by:

$$c = \frac{\omega}{k} = \sqrt{\frac{g}{k}\tanh(kH)} = \sqrt{\frac{g\lambda}{2\pi}\tanh\left(\frac{2\pi H}{\lambda}\right)}. \tag{7.29}$$

This result is of fundamental importance for water waves. It shows that surface waves are *dispersive* because their propagation speed depends on wave number, with lower k (longer wavelength) waves traveling faster. (*Dispersion* is a term borrowed from optics, where it signifies separation of different colors due to the speed of light in a medium depending on the wavelength.) Thus, a concentrated wave packet made up of many different wavelengths (or frequencies) will not maintain a constant waveform or shape. Instead, it will disperse or spread out as it travels. The longer wavelength components will travel faster than the shorter wavelength ones so that an initial impulse evolves into a wide wave train. This is precisely what happens when an object is dropped onto the surface of a quiescent pool, pond, or lake. The radial extent of the circular waves increases with time, and the longest wavelengths appear farthest from the point of impact while the shortest wavelengths are seen closest to the point of impact.

The rest of this section covers some implications of the linear surface-wave solution (7.26) and the dispersion relation (7.28). Given the ease with which it can be measured, the pressure below the liquid surface is considered first. In particular, the time-dependent perturbation pressure,

$$p' \equiv p + \rho g z, \tag{7.30}$$

produced by surface waves is of interest. Using this and (7.26) in the linearized Bernoulli equation (7.20) leads to

$$p' = -\rho\frac{\partial\phi}{\partial t} = \rho\,\frac{a\omega^2}{k}\,\frac{\cosh(k(z+H))}{\sinh(kH)}\cos(kx-\omega t) = \rho g a\,\frac{\cosh(k(z+H))}{\cosh(kH)}\cos(kx-\omega t), \tag{7.31}$$

where the second equality follows when (7.28) is used to eliminate ω^2. The perturbation pressure therefore decreases with increasing depth, and the extent of this decrease depends on the wavelength through k.

Another interesting feature of linear surface waves is the fact that they travel and cause fluid elements to move, but they do not cause fluid elements to travel. To ascertain what happens when a linear surface wave passes, consider the fluid element that follows a path $\mathbf{x}_p(t) = x_p(t)\mathbf{e}_x + z_p(t)\mathbf{e}_z$. The path-line equations (3.8) for this fluid element are

$$\frac{dx_p(t)}{dt} = u(x_p, z_p, t), \text{ and } \frac{dz_p(t)}{dt} = w(x_p, z_p, t), \tag{7.32}$$

which imply:

$$\frac{dx_p}{dt} = a\omega \frac{\cosh\big(k(z_p + H)\big)}{\sinh(kH)} \cos(kx_p - \omega t), \text{ and } \frac{dz_p}{dt} = a\omega \frac{\sinh\big(k(z_p + H)\big)}{\sinh(kH)} \sin(kx_p - \omega t), \quad (7.33)$$

when combined with (7.27). To be consistent with the small amplitude approximation, these equations can be linearized by setting $x_p(t) = x_0 + \xi(t)$ and $z_p(t) = z_0 + \zeta(t)$, where (x_0, z_0) is the average fluid element location and the element excursion vector (ξ, ζ) (see Figure 7.3) is assumed to be small compared to the wavelength. Thus, the linearized versions of (7.33) are obtained by evaluating the right side of each equation at (x_0, z_0):

$$\frac{d\xi}{dt} \cong a\omega \frac{\cosh(k(z_0 + H))}{\sinh(kH)} \cos(kx_0 - \omega t), \text{ and } \frac{d\zeta}{dt} \cong a\omega \frac{\sinh(k(z_0 + H))}{\sinh(kH)} \sin(kx_0 - \omega t), \quad (7.34a, 7.34b)$$

where x_0 and z_0 have been assumed independent of time. This linearization is valid when the velocity of the fluid element along its path is nearly equal to the fluid velocity at (x_0, z_0) at that instant. It is accurate when $a \ll \lambda$. The equations (7.34a, 7.34b) are reminiscent of those in Example 3.1, and are readily time-integrated:

$$\xi \cong -a \frac{\cosh(k(z_0 + H))}{\sinh(kH)} \sin(kx_0 - \omega t), \text{ and } \zeta \cong a \frac{\sinh(k(z_0 + H))}{\sinh(kH)} \cos(kx_0 - \omega t). \quad (7.35a, 7.35b)$$

Here we note that $\xi(t)$ and $\zeta(t)$ are entirely oscillatory. Neither contains a term that increases with time so the assumption that x_0 and z_0 are time independent is self consistent when $a \ll \lambda$. Elimination of the phase $(kx_0 - \omega t)$ from (7.35a, 7.35b) gives:

$$\xi^2 \Big/ \left[a \frac{\cosh(k(z_0 + H))}{\sinh(kH)}\right]^2 + \zeta^2 \Big/ \left[a \frac{\sinh(k(z_0 + H))}{\sinh(kH)}\right]^2 = 1, \quad (7.36)$$

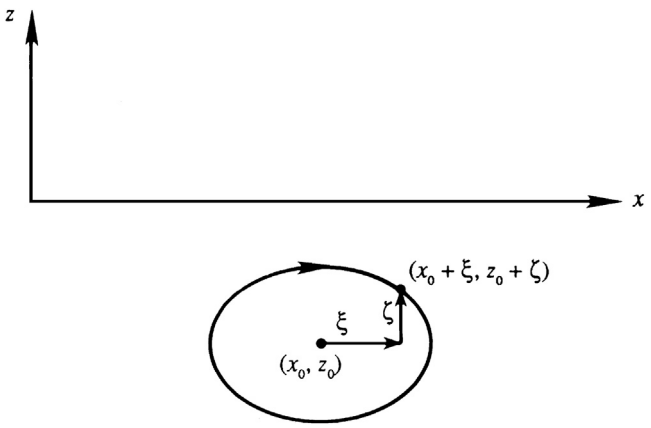

FIGURE 7.3 Orbit of a fluid particle below a linear surface wave. The average position of the particle is (x_0, z_0), and $\xi(t)$ and $\zeta(t)$ are small time-dependent displacements in the horizontal and vertical directions, respectively. When the surface wave is sinusoidal, travels to the right, and has small amplitude, the fluid particles below the surface traverse closed elliptical orbits in the clockwise direction.

which represents an ellipse. Both the semi-major axis, $a\cosh[k(z_0 + H)]/\sinh(kH)$, and the semi-minor axis, $a\sinh[k(z_0 + H)]/\sinh(kH)$, decrease with depth, with the minor axis vanishing at $z_0 = -H$ (Figure 7.4b). The distance between foci remains constant with depth. Equations (7.35a, 7.35b) show that the phase of the motion is independent of z_0, so fluid elements in any vertical column move in phase. That is, if one of them is at the top of its orbit, then all elements at the same x_0 are at the top of their orbits.

Streamlines may be found from the stream function ψ, which can be determined by integrating the velocity component equations $\partial\psi/\partial z = u$ and $-\partial\psi/\partial x = w$ when u and w are given by (7.27):

$$\psi = \frac{a\omega}{k}\frac{\sinh(k(z+H))}{\sinh(kH)}\cos(kx - \omega t) \tag{7.37}$$

(Exercise 7.4). To understand the streamline structure, consider a particular time, $t = 0$, when

$$\psi \propto \sin k(z+H)\cos kx.$$

It is clear that $\psi = 0$ at $z = -H$, so that the bottom wall is a part of the $\psi = 0$ streamline. However, ψ is also zero at $kx = \pm\pi/2, \pm 3\pi/2, \ldots$ for any z. At $t = 0$ and at these values of kx, η from (7.2) vanishes. The resulting streamline pattern is shown in Figure 7.5. It is seen that the *velocity is in the direction of propagation* (*and horizontal*) *at all depths below the crests*, *and opposite to the direction of propagation at all depths below troughs*.

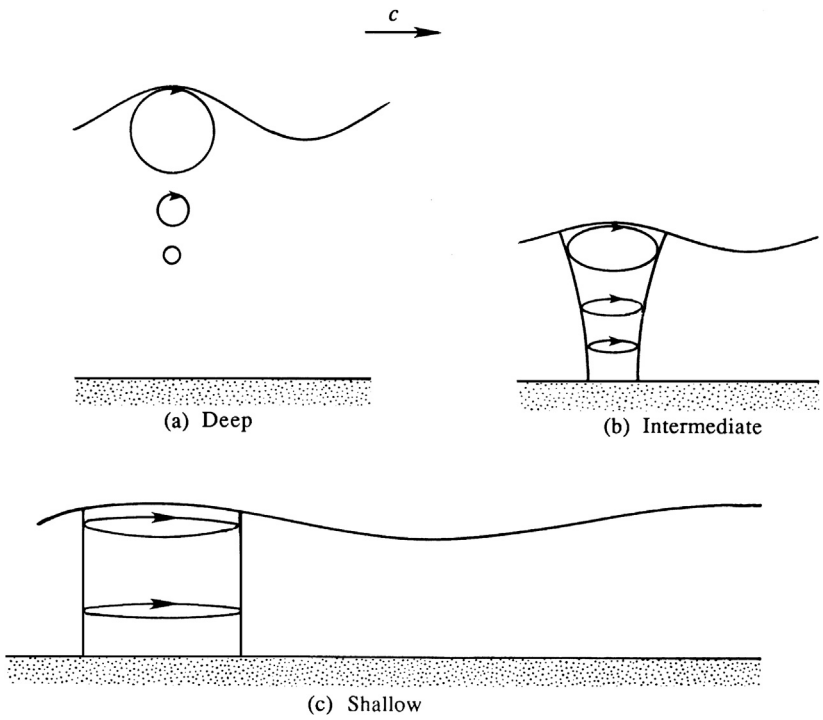

FIGURE 7.4 Fluid particle orbits caused by a linear sinusoidal surface wave traveling to the right for three liquid depths. (a) When the liquid is deep and $\tanh(kH) \approx 1$, then particle orbits are circular and decrease in size with increasing depth. (b) At intermediate depths, the particle orbits are broad ellipses that narrow and contract with increasing depth. (c) When the water is shallow and $\tanh(kH) \approx \sinh(kH) \approx kH$, the orbits are thin ellipses that become thinner with increasing depth.

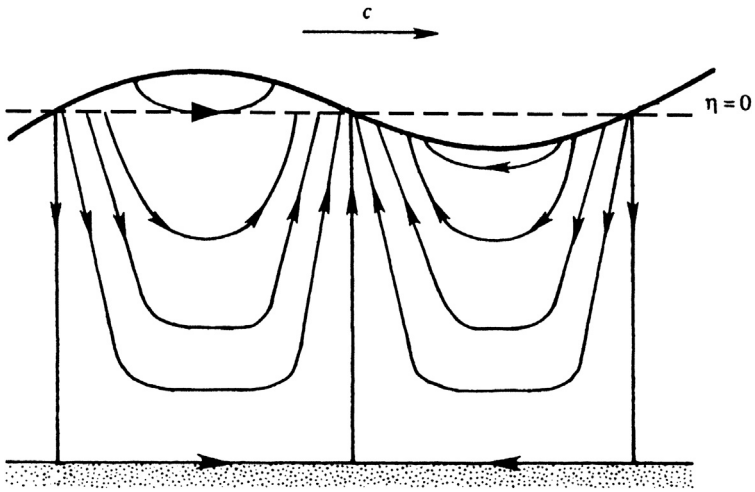

FIGURE 7.5 Instantaneous streamline pattern for a sinusoidal surface wave propagating to the right. Here the $\psi = 0$ streamline follows the bottom and jumps up to contact the surface where $\eta = 0$. The remaining streamlines start and end on the liquid surface with purely horizontal motion found in the $+x$ direction below a wave crest and in $-x$ direction below a wave trough.

Surface gravity waves possess kinetic energy in the motion of the fluid and potential energy in the vertical deformation of the free surface. The kinetic energy per unit horizontal area, E_k, is found by integrating over the depth and averaging over a wavelength:

$$E_k = \frac{\rho}{2\lambda}\int_0^\lambda \int_{-H}^0 (u^2 + w^2)\, dz\, dx.$$

Here the z-integral is taken from $z = -H$ to $z = 0$, consistent with the linearization performed to reach (7.26); integrating from $z = -H$ to $z = \eta$ merely introduces a higher-order term. Substitution of the velocity components from (7.27) gives:

$$E_k = \frac{\rho\omega^2}{2\sinh^2 kH}\left[\frac{1}{\lambda}\int_0^\lambda a^2\cos^2(kx - \omega t)\, dx \int_{-H}^0 \cosh^2 k(z+H)\, dz + \frac{1}{\lambda}\int_0^\lambda a^2\sin^2(kx - \omega t)\, dx \int_{-H}^0 \sinh^2 k(z+H)\, dz\right]. \tag{7.38}$$

In terms of free-surface displacement η, the x-integrals in (7.38) can be written as

$$\frac{1}{\lambda}\int_0^\lambda a^2\cos^2(kx - \omega t)\, dx = \frac{1}{\lambda}\int_0^\lambda a^2\sin^2(kx - \omega t)\, dx = \frac{1}{\lambda}\int_0^\lambda \eta^2 dx = \overline{\eta^2},$$

where $\overline{\eta^2}$ is the mean-square vertical surface displacement. The z-integrals in (7.38) are easy to evaluate by expressing the hyperbolic functions in terms of exponentials. Using the dispersion relation (7.28), (7.38) finally becomes

$$E_k = \frac{1}{2}\rho g\overline{\eta^2}, \tag{7.39}$$

which is the kinetic energy of the wave motion per unit horizontal area.

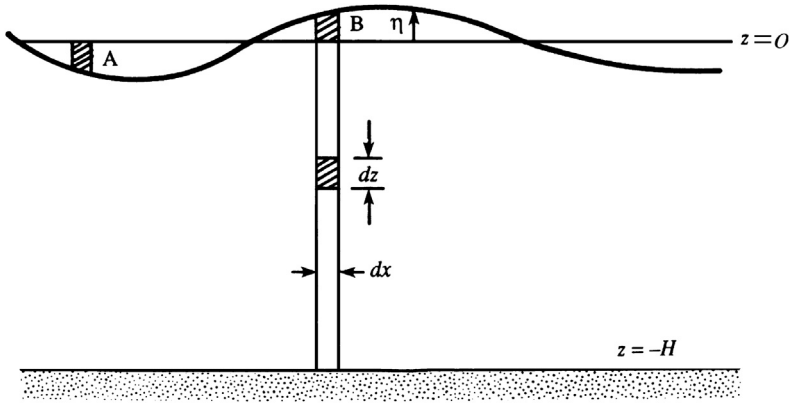

FIGURE 7.6 Calculation of potential energy of a fluid column. Here work must be done to push the liquid surface down below $z = 0$ (A), and lift the liquid surface up above $z = 0$ (B).

The *potential energy* E_p of the wave system is defined as the work done per unit area to deform a horizontal free surface into the disturbed state. It is therefore equal to the *difference* of potential energies of the system in the disturbed and undisturbed states. As the potential energy of an element in the fluid (per unit length in y) is $\rho g z\, dx\, dz$ (Figure 7.6), E_p can be calculated as

$$E_p = \frac{\rho g}{\lambda}\int_0^{\lambda}\int_{-H}^{\eta} z\, dz\, dx - \frac{\rho g}{\lambda}\int_0^{\lambda}\int_{-H}^{0} z\, dz\, dx, = \frac{\rho g}{\lambda}\int_0^{\lambda}\int_{0}^{\eta} z\, dz\, dx = \frac{\rho g}{2\lambda}\int_0^{\lambda}\eta^2 dx. \tag{7.40}$$

(An easier way to arrive at the expression for E_p is to note that the potential energy increase due to wave motion equals the work done in raising column A in Figure 7.6 to the location of column B, and integrating over *half the wavelength*. This is because an interchange of A and B over half a wavelength automatically forms a complete wavelength of the deformed surface. The mass (per unit length in y) of column A is $\rho\eta dx$, and the center of gravity is raised by η when A is taken to B. This agrees with the last form in (7.40).) Equation (7.40) can also be written in terms of the mean square displacement as

$$E_p = \frac{1}{2}\rho g\overline{\eta^2}. \tag{7.41}$$

Thus, the average kinetic and potential energies are equal. This is called the *principle of equipartition of energy* and is valid in conservative dynamical systems undergoing small oscillations that are unaffected by planetary rotation. However, it is not valid when Coriolis forces are included, as described in Chapter 13. The total wave energy in the water column per unit horizontal area is

$$E = E_p + E_k = \rho g\overline{\eta^2} = \frac{1}{2}\rho g a^2, \tag{7.42}$$

where the last form in terms of the amplitude a is valid if η is assumed sinusoidal, since the average over a wavelength of the square of a sinusoid is ½.

Next, consider the rate of transmission of energy due to a single sinusoidal component of wave number k. The *energy flux* across the vertical plane $x = 0$ is the pressure work done by

the fluid in the region $x < 0$ on the fluid in the region $x > 0$. The time average energy flux F per unit length of crest is (writing p as the sum of a perturbation p' and a background pressure $-\rho g z$):

$$F = \left\langle \int_{-H}^{0} pu\, dz \right\rangle = \left\langle \int_{-H}^{0} p'u\, dz \right\rangle - \rho g \langle u \rangle \int_{-H}^{0} z\, dz = \left\langle \int_{-H}^{0} p'u\, dz \right\rangle, \tag{7.43}$$

where $\langle\ \rangle$ denotes an average over a wave period, and we have used the fact that $\langle u \rangle = 0$. Substituting for p' from (7.31) and u from (7.28), (7.43) becomes

$$F = \langle \cos^2 (kx - \omega t) \rangle \frac{\rho a^2 \omega^3}{k \sinh^2 kH} \int_{-H}^{0} \cosh^2 k(z + H)\, dz.$$

The time average of $\cos^2(kx - \omega t)$ is ½, and the z-integral can be carried out by writing it in terms of exponentials, thus

$$F = \left[\frac{1}{2}\rho g a^2\right]\left[\frac{c}{2}\left(1 + \frac{2kH}{\sinh 2kH}\right)\right]. \tag{7.44}$$

The first factor is the wave energy per unit area given in (7.42). Therefore, the second factor must be the speed of propagation of the wave energy of component k. This energy propagation speed is called the *group speed*, and is further discussed in Section 7.5.

Approximations for Deep and Shallow Water

The preceding analysis is applicable for any value of H/λ. However, interesting simplifications are provided in the next few paragraphs for deep water, $H/\lambda \gg 1$, and shallow water, $H/\lambda \ll 1$.

Consider deep water first. The general expression for phase speed is (7.29), but we know that $\tanh(x) \to 1$ for $x \to \infty$ (Figure 7.7). However, x need not be very large for this approximation to be valid, because $\tanh(x) = 0.96403$ for $x = 2.0$. It follows that, with 2% accuracy, (7.29) can be approximated by

$$c = \sqrt{g/k} = \sqrt{g\lambda/2\pi} \tag{7.45}$$

for $H > 0.32\lambda$ (corresponding to $kH > 2.0$). Surface waves are therefore classified as *deep-water waves* if the depth is more than one-third of the wavelength. Here, it is clear that deep-water waves are dispersive since their phase speed depends on wavelength.

A dominant period of wind-generated surface gravity waves in the ocean is ~10 s, which, via the dispersion relation (7.28), corresponds to a wavelength of 150 m. The water depth on a typical continental shelf is ~100 m, and in the open ocean it is ~4 km. Thus, the dominant wind waves in the ocean, even over the continental shelf, act as deep-water waves and do not feel the effects of the ocean bottom until they arrive near a coastline. This is not true of the very long wavelength gravity waves or tsunamis generated by tidal forces or earthquakes. Such waves may have wavelengths of hundreds of kilometers.

In deep water, the semi-major and semi-minor axes of particle orbits produced by small-amplitude gravity waves are nearly equal to ae^{kz} since

$$\frac{\cosh(k(z+H))}{\sinh(kH)} \approx \frac{\sinh(k(z+H))}{\sinh(kH)} \approx e^{kz}$$

for $kH > 2.0$, so the deep-water wave-induced fluid particle motions are:

$$\xi \cong -ae^{kz_0}\sin(kx_0 - \omega t), \text{ and } \zeta \cong ae^{kz_0}\cos(kx_0 - \omega t). \tag{7.46}$$

The orbits are circles (Figure 7.4a). At the surface, their radius is a, the amplitude of the wave.

The fluid velocity components for deep-water waves are

$$u = a\omega e^{kz}\cos(kx - \omega t), \text{ and } w = a\omega e^{kz}\sin(kx - \omega t). \tag{7.47}$$

At a fixed spatial location, the velocity vector rotates clockwise (for a wave traveling in the positive x direction) at frequency ω, while its magnitude remains constant at $a\omega e^{kz}$.

For deep-water waves, the perturbation pressure from (7.31) simplifies to

$$p' = \rho g a e^{kz}\cos(kx - \omega t), \tag{7.48}$$

which shows the wave-induced pressure change decays exponentially with depth, reaching 4% of its surface magnitude at a depth of $\lambda/2$. Thus, a bottom-mounted sensor used to record

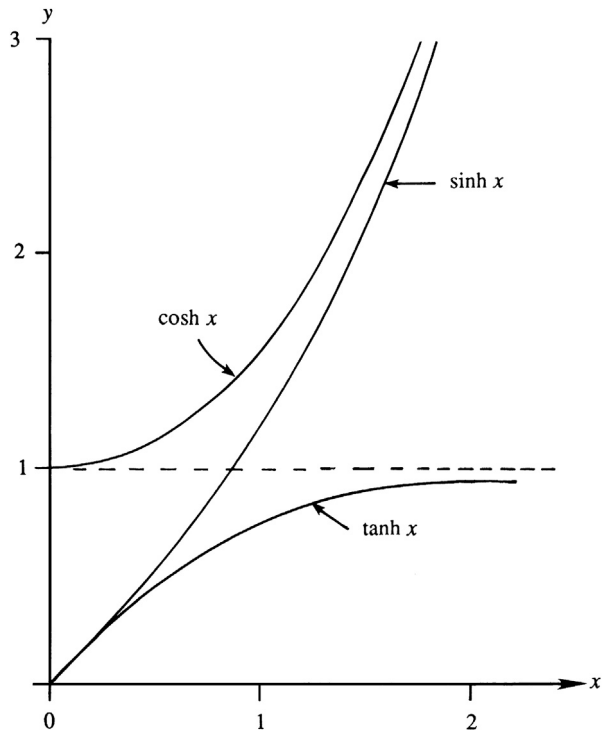

FIGURE 7.7 Behavior of hyperbolic functions $\cosh(x)$, $\sinh(x)$, and $\tanh(x)$ vs. x. For small x, $\cosh(x) \approx 1$ and $\sinh(x) \approx \tanh(x) \approx x$. For large x, $\cosh(x) \approx \sinh(x)$ and $\tanh(x) \approx 1$.

wave-induced pressure fluctuations will respond as a low-pass filter. Its signal will favor long waves while rejecting short ones.

The shallow water limit is also important and interesting. We know that $\tanh(x) \approx x$ as $x \to 0$ (Figure 7.7), so for $H/\lambda \ll 1$:

$$\tanh(2\pi H/\lambda) \approx 2\pi H/\lambda,$$

in which case the phase speed from (7.29) simplifies to

$$c = \sqrt{gH}, \tag{7.49}$$

and this matches the control volume result from Example 4.3. The approximation gives better than 3% accuracy if $H < 0.07\lambda$. Therefore, surface waves are regarded as *shallow-water waves* only if they are 14 times longer than the water depth. For these waves, (7.49) shows that the wave speed increases with water depth, and that it is independent of wavelength, so shallow-water waves are *nondispersive*.

To determine the approximate form of particle orbits for shallow-water waves, substitute the following approximations into (7.35):

$$\cosh(k(z+H)) \cong 1, \ \sinh(k(z+H)) \cong k(z+H), \text{ and } \sinh(kH) \cong kH.$$

The particle excursions then become

$$\xi \cong -\frac{a}{kH}\sin(kx_0 - \omega t), \text{ and } \zeta \cong a\left(1+\frac{z}{H}\right)\cos(kx_0 - \omega t). \tag{7.50}$$

These represent thin ellipses (Figure 7.4c), with a depth-independent semi-major axis a/kH and a semi-minor axis $a(1 + z/H)$ that linearly decreases to zero at the bottom wall.

From (7.27), the velocity field is

$$u = \frac{a\omega}{kH}\cos(kx - \omega t), \text{ and } w = a\omega\left(1+\frac{z}{H}\right)\sin(kx - \omega t), \tag{7.51}$$

which shows that the vertical component is much smaller than the horizontal component.

The pressure change from the undisturbed state is found from (7.31) to be

$$p' = \rho g a \cos(kx - \omega t) = \rho g \eta, \tag{7.52}$$

where (7.2) has been used to express the pressure change in terms of η. This shows that the pressure change at any point is independent of depth, and equals the hydrostatic increase of pressure due to the surface elevation change η. *The pressure field is therefore completely hydrostatic in shallow-water waves*. Vertical accelerations are negligible because of the small w-field. For this reason, shallow water waves are also called *hydrostatic waves*. Any worthwhile pressure sensor mounted on the bottom will sense these waves.

The depth-dependent wave speed (7.49) in shallow water leads to the phenomenon of shallow-water wave *refraction* observed at coastlines around the world. Consider a sloping beach, with depth contours parallel to the coastline (Figure 7.8). Assume that waves are propagating toward the coast from the deep ocean, with their crests at an angle to the coastline. Sufficiently near the coastline they begin to feel the effect of the bottom and finally become shallow-water waves. Their frequency does not change along the path, but their speed of propagation $c = (gH)^{1/2}$ and their wavelength λ become smaller. Consequently, the crest

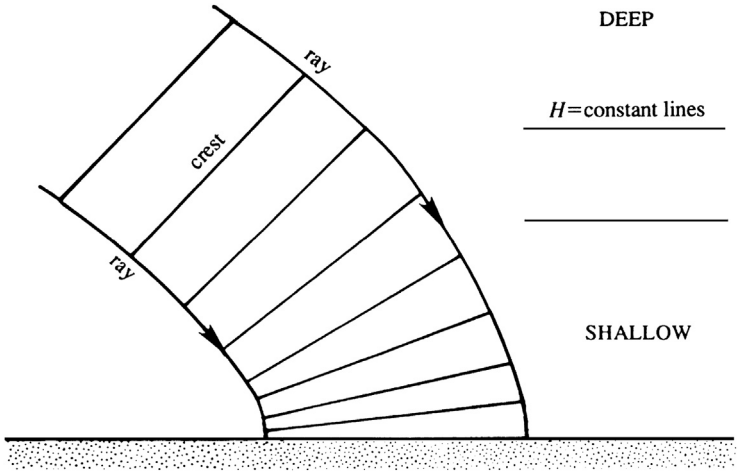

FIGURE 7.8 Refraction of a surface gravity wave approaching a sloping beach caused by changes in depth. In deep water, wave crests are commonly misaligned with isobaths. However, as a wave approaches the shore from any angle, the portion of the wave in shallower water will be slowed compared to that in deeper water. Thus, the wave crests will rotate and tend to become parallel to the shore as they approach it.

lines, which are perpendicular to the local direction of c, tend to become parallel to the coast. This is why the waves coming toward a gradually sloping beach always seem to have their crests parallel to the coastline.

An interesting example of wave refraction occurs when a deep-water wave train with straight crests approaches an island (Figure 7.9). Assume that the water gradually becomes shallower as the island is approached, and that the constant depth contours are circles

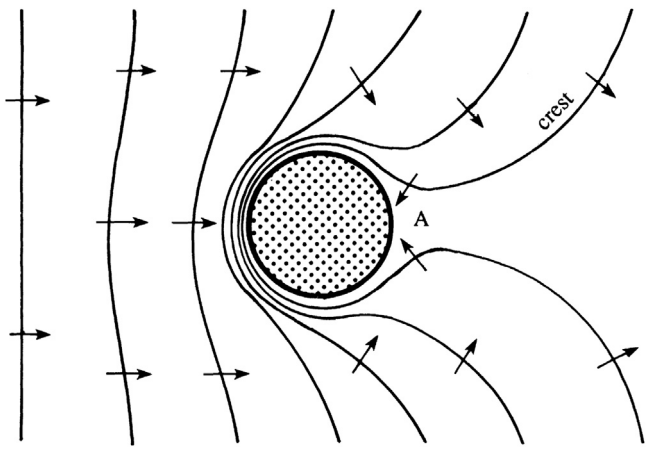

FIGURE 7.9 Refraction of surface gravity waves approaching a circular island with a gradually sloping beach. Crest lines are shown and are observed to travel toward the island, even on its shadow side A. *Reprinted with the permission of Mrs. Dorothy Kinsman Brown: B. Kinsman,* Wind Waves, *Prentice-Hall, Englewood Cliffs, NJ, 1965.*

concentric with the island. Figure 7.9 shows that the waves always come in *toward* the island, even on the shadowed-side marked A.

The bending of wave paths in an inhomogeneous medium is called *wave refraction*. In this case the source of inhomogeneity is the spatial dependence of H. The analogous phenomenon in optics is the bending of light due to density changes in its path.

7.3. INFLUENCE OF SURFACE TENSION

As described in Section 1.6, the interface between two immiscible fluids is in a state of tension. The tension acts as another restoring force on surface deformation, enabling the interface to support waves in a manner analogous to waves on a stretched membrane or string. Waves due to the presence of surface tension are called *capillary waves*. Although gravity is not needed to support these waves, the existence of surface tension alone without gravity is uncommon in terrestrial environments. Thus, the preceding results for pure gravity waves are modified to include surface tension in this section.

As shown in Section 4.10, there is a pressure difference Δp across a curved interface with nonzero surface tension σ. When the surface's principal radii of curvature are R_1 and R_2, this pressure difference is

$$\Delta p = \sigma(1/R_1 + 1/R_2), \tag{1.5}$$

where the pressure is greater on the side of the surface with the centers of curvature of the interface. This pressure difference modifies the free-surface boundary condition (7.19).

For straight-crested surface waves that produce fluid motion in the x-z plane, there is no variation in the y direction, so one of the radii of curvature is infinite, and the other, denoted R, lies in the x-z plane. Thus, if the pressure above the liquid is atmospheric, p_a, then pressure p in the liquid at the surface $z = \eta$ can be found from (1.5):

$$p_a - (p)_{z=\eta} = \sigma\frac{1}{R} = \sigma\frac{\partial^2\eta/\partial x^2}{\left[1 + (\partial\eta/\partial x)^2\right]^{3/2}} \cong \sigma\frac{\partial^2\eta}{\partial x^2}, \tag{7.53}$$

where the second equality follows from the definition of the curvature $1/R$ and the final approximate equality holds when the liquid surface slope $\partial\eta/\partial x$ is small. As before we can choose p to be a gauge pressure and this means setting $p_a = 0$ in (7.53), which leaves

$$(p)_{z=\eta} = -\sigma\frac{\partial^2\eta}{\partial x^2}, \tag{7.54}$$

as the pressure-matching boundary condition at the liquid surface for small-slope surface waves. As before, this can be combined with the linearized unsteady Bernoulli equation (7.20) and evaluated on $z = 0$ for small-slope surface waves:

$$\left(\frac{\partial\phi}{\partial t}\right)_{z=0} = \frac{\sigma}{\rho}\frac{\partial^2\eta}{\partial x^2} - g\eta. \tag{7.55}$$

The linear capillary-gravity, surface-wave solution now proceeds in an identical manner to that for pure gravity waves, except that the pressure boundary condition (7.21) is replaced by

(7.55). This modification only influences the dispersion relation $\omega(k)$, which is found by substitution of (7.2) and (7.26) into (7.55), to give

$$\omega = \sqrt{k\left(g + \frac{\sigma k^2}{\rho}\right)\tanh(kH)}, \tag{7.56}$$

so the phase velocity is

$$c = \sqrt{\left(\frac{g}{k} + \frac{\sigma k}{\rho}\right)\tanh kH} = \sqrt{\left(\frac{g\lambda}{2\pi} + \frac{2\pi\sigma}{\rho\lambda}\right)\tanh\frac{2\pi H}{\lambda}}. \tag{7.57}$$

A plot of (7.57) is shown in Figure 7.10. The primary effect of surface tension is to increase c above its value for pure gravity waves at all wavelengths. This increase occurs because there are two restoring forces that act together on the surface, instead of just one. However, the effect of surface tension is only appreciable for small wavelengths. The nominal size of these wavelengths is obtained by noting that there is a minimum phase speed at $\lambda = \lambda_m$, and surface tension dominates for $\lambda < \lambda_m$ (Figure 7.10). Setting $dc/d\lambda = 0$ in (7.57), and assuming deep water, $H > 0.32\lambda$ so $\tanh(2\pi H/\lambda) \approx 1$, produces:

$$c_{\min} = \left[\frac{4g\sigma}{\rho}\right]^{1/4} \quad \text{at} \quad \lambda_m = 2\pi\sqrt{\frac{\sigma}{\rho g}}. \tag{7.58}$$

For an air-water interface at 20°C, the surface tension is $\sigma = 0.073$ N/m, giving

$$c_{\min} = 23.1 \text{ cm/s} \quad \text{at} \quad \lambda_m = 1.71 \text{ cm}. \tag{7.59}$$

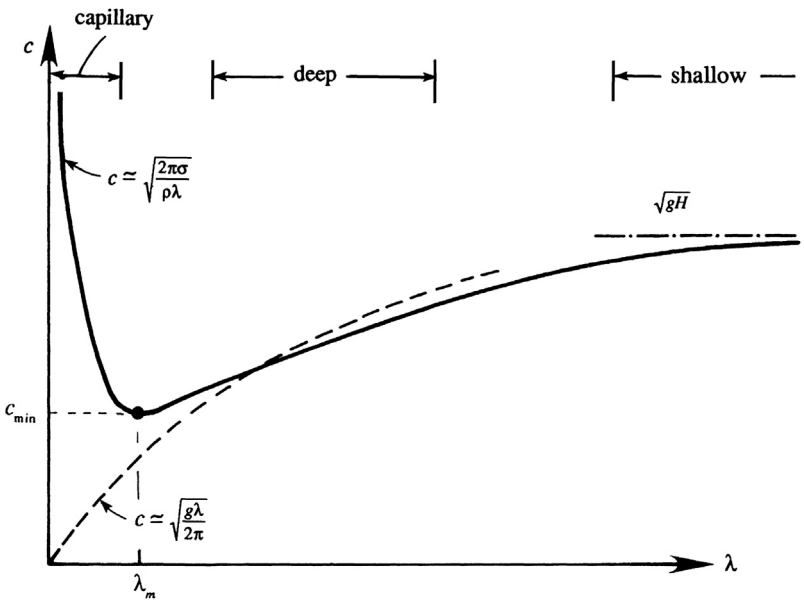

FIGURE 7.10 Generic sketch of the phase velocity c vs. wavelength λ for waves on the surface of liquid layer of depth H. The phase speed of the shortest waves is set by the liquid's surface tension σ and density ρ. The phase speed of the longest waves is set by gravity g and depth H. In between these limits, the phase speed has a minimum that typically occurs when the effects of surface tension and gravity are both important.

Therefore, only short-wavelength waves ($\lambda < \sim 7$ cm for an air-water interface), called *ripples*, are affected by surface tension. The waves specified by (7.59) are readily observed as the wave rings closest to the point of impact after an object is dropped onto the surface of a quiescent pool, pond, or lake of clean water. Surfactants and surface contaminants may lower σ or even introduce additional surface properties like surface viscosity or elasticity. Water surface wavelengths below 4 mm are dominated by surface tension and are essentially unaffected by gravity. From (7.57), the phase speed of *pure capillary waves* is

$$c = \sqrt{\frac{2\pi\sigma}{\rho\lambda}}, \tag{7.60}$$

where again $\tanh(2\pi H/\lambda) \approx 1$ has been assumed.

7.4. STANDING WAVES

The wave motion results presented so far are for one propagation direction ($+x$) as specified by (7.2). However, a small-amplitude sinusoidal wave with phase ($kx + \omega t$) is an equally valid solution of (7.11). Such a waveform,

$$\eta(x,t) = a\cos[kx + \omega t], \tag{7.61}$$

only differs from (7.2) in its direction of propagation. Its wave crests move in the $-x$ direction with increasing time. Interestingly, nonpropagating waves can be generated by superposing two waves with the same amplitude and wavelength that move in opposite directions. The resulting surface displacement is

$$\eta = a\cos(kx - \omega t) + a\cos(kx + \omega t) = 2a\cos kx\cos\omega t.$$

Here it follows that $\eta = 0$ at $kx = \pm\pi/2$, $\pm 3\pi/2$, etc., for all time. Such locations of zero surface displacement are called *nodes*. In this case, deflections of the liquid surface do not travel. The surface simply oscillates up and down at frequency ω with a spatially varying amplitude, keeping the nodal points fixed. Such waves are called *standing waves*. The corresponding stream function, a direct extension of (7.37), includes both the $\cos(kx - \omega t)$ and $\cos(kx + \omega t)$ components:

$$\psi = \frac{a\omega}{k}\frac{\sinh k(z+H)}{\sinh kH}[\cos(kx - \omega t) - \cos(kx + \omega t)] = \frac{2a\omega}{k}\frac{\sinh k(z+H)}{\sinh kH}\sin kx\sin\omega t. \tag{7.62}$$

The instantaneous streamline pattern shown in Figure 7.11 should be compared with the streamline pattern for a propagating wave (Figure 7.5).

Standing waves may form in a limited body of water such as a tank, pool, or lake when traveling waves reflect from its walls, sides, or shores. A standing-wave oscillation in a lake is called a *seiche* (pronounced "saysh"), in which only certain wavelengths and frequencies ω (eigenvalues) are allowed by the system. Consider a lake of length L with uniform depth H and vertical shores (walls), and assume that the waves are invariant along y. The possible wavelengths are found by setting $u = 0$ at the two walls. Here, $u = \partial\psi/\partial z$, so (7.62) gives

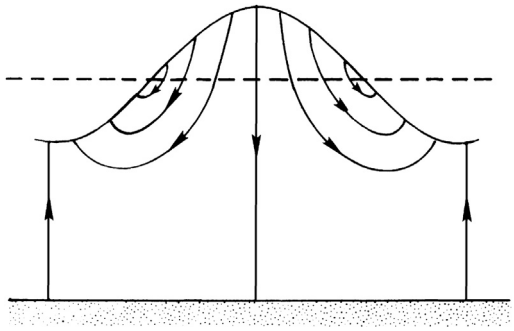

FIGURE 7.11 Instantaneous streamline pattern in a standing surface gravity wave. Here the $\psi = 0$ streamline follows the bottom and jumps up to contact the surface at wave crests and troughs where the horizontal velocity is zero. If this standing wave represents the $n = 0$ mode of a reservoir of length L with vertical walls, then $L = \lambda/2$ is the distance between a crest and a trough. If it represents the $n = 1$ mode, then $L = \lambda$ is the distance between successive crests or successive troughs.

$$u = 2a\omega \frac{\cosh k(z+H)}{\sinh kH} \sin kx \sin \omega t. \tag{7.63}$$

Taking the walls at $x = 0$ and L, the condition of no flow through the walls requires $\sin(kL) = 0$, that is,

$$kL = (n+1)\pi \quad n = 0, 1, 2, \ldots,$$

which gives the allowable wavelengths as

$$\lambda = \frac{2L}{n+1}. \tag{7.64}$$

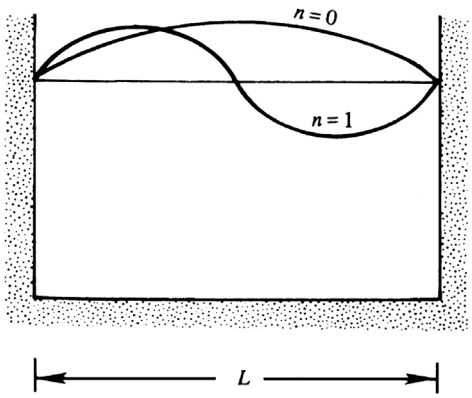

FIGURE 7.12 Distributions of horizontal velocity u for the first two normal modes in a lake or reservoir with vertical sides. Here the boundary conditions require $u = 0$ on the vertical sides. These distributions are consistent with the streamline pattern of Figure 7.11.

The largest possible wavelength is $2L$ and the next smaller is L (Figure 7.12). The allowed frequencies can be found from the dispersion relation (7.28), giving

$$\omega = \sqrt{\frac{\pi g(n+1)}{L}\tanh\left[\frac{(n+1)\pi H}{L}\right]}, \tag{7.65}$$

which are the natural frequencies of the lake.

7.5. GROUP VELOCITY, ENERGY FLUX, AND DISPERSION

A variety of interesting phenomena take place when waves are dispersive and their phase speed depends on wavelength. Such wavelength-dependent propagation is common for waves that travel on interfaces between different materials (Graff, 1975). Examples are Rayleigh waves (vacuum and a solid), Stonely waves (a solid and another material), or interface waves (two different immiscible liquids). Here we consider only air-water interface waves and emphasize deep-water gravity waves for which c is proportional to $\sqrt{\lambda}$.

In a dispersive system, the energy of a wave component does not propagate at the phase velocity $c = \omega/k$, but at the *group velocity* defined as $c_g = d\omega/dk$. To understand this, consider the superposition of two sinusoidal wave components of equal amplitude but slightly different wave number (and consequently slightly different frequency because $\omega = \omega(k)$). The waveform of the combination is

$$\eta = a\cos(k_1 x - \omega_1 t) + a\cos(k_2 x - \omega_2 t).$$

Applying the trigonometric identity for the sum of cosines of different arguments, we obtain

$$\eta = 2a\cos\left(\frac{1}{2}\Delta k x - \frac{1}{2}\Delta\omega x\right)\cos(kx - \omega t), \tag{7.66}$$

where $\Delta k = k_2 - k_1$ and $\Delta\omega = \omega_2 - \omega_1$, $k = (k_1 + k_2)/2$, and $\omega = (\omega_1 + \omega_2)/2$. Here, $\cos(kx - \omega t)$ is a progressive wave with a phase speed of $c = \omega/k$. However, its amplitude $2a$ is modulated by a *slowly varying* function $\cos[\Delta k x/2 - \Delta\omega t/2]$, which has a large wavelength $4\pi/\Delta k$, a long period $4\pi/\Delta\omega$, and propagates at a speed (wavelength/period) of

$$c_g = \Delta\omega/\Delta k = d\omega/dk, \tag{7.67}$$

where the second equality holds in the limit as Δk and $\Delta\omega \to 0$. Multiplication of a rapidly varying sinusoid and a slowly varying sinusoid, as in (7.66), generates repeating wave groups (Figure 7.13). The individual wave crests (and troughs) propagate with the speed $c = \omega/k$, but the envelope of the wave groups travels with the speed c_g, which is therefore called the *group velocity*. If $c_g < c$, then individual wave crests appear spontaneously at a nodal point, proceed forward through the wave group, and disappear at the next nodal point. If, on the other hand, $c_g > c$, then individual wave crests emerge from a forward nodal point and vanish at a backward nodal point.

Equation (7.67) shows that the group speed of waves of a certain wave number k is given by the slope of the *tangent* to the dispersion curve $\omega(k)$. In contrast, the phase velocity is given by the slope of the radius or distance vector on the same plot (Figure 7.14).

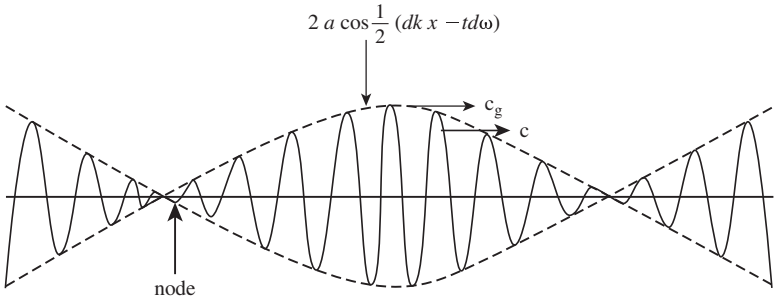

FIGURE 7.13 Linear combination of two equal amplitude sinusoids of nearly the same frequency that form a modulated wave train. Individual wave crests or troughs travel at the phase speed. However, the nodal locations which partition the wave train into groups, travel at the group speed.

A particularly illuminating example of the idea of group velocity is provided by the concept of a *wave packet*, formed by combining all wave numbers in a certain narrow band δk around a central value k. In physical space, the wave appears nearly sinusoidal with wavelength $2\pi/k$, but the amplitude *dies away* over a distance proportional to $1/\delta k$ (Figure 7.15). If the spectral width δk is narrow, then decay of the wave amplitude in physical space is slow. The concept of such a wave packet is more realistic than the one in Figure 7.13, which is rather unphysical because the wave groups repeat themselves. Suppose that, at some initial time, the wave group is represented by

$$\eta = a(x)\cos kx.$$

It can be shown (see, for example, Phillips, 1977, p. 25) that for small times, the subsequent evolution of the wave profile is approximately described by

$$\eta = a(x - c_g t)\cos(kx - \omega t), \tag{7.68}$$

where $c_g = d\omega/dk$. This shows that the *amplitude of a wave packet travels with the group speed*. It follows that c_g must equal the speed of propagation of *energy* of a certain wavelength. The fact

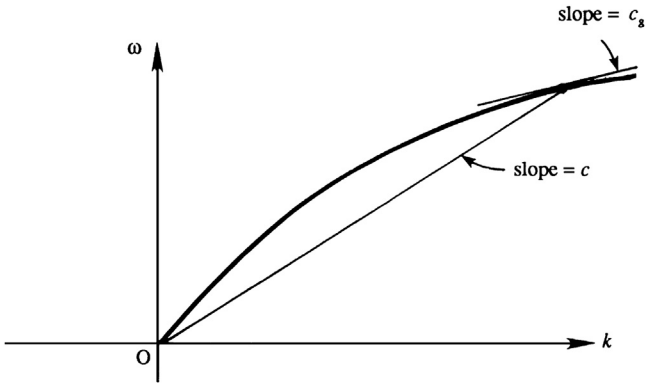

FIGURE 7.14 Graphical depiction of the phase speed, c, and group speed, c_g, on a generic plot of a gravity wave dispersion relation, $\omega(k)$ vs. k. If a sinusoidal wave has frequency ω and wave number k, then the phase speed c is the slope of the straight line through the points (0, 0) and (k, ω), while the group speed c_g is the tangent to the dispersion relation at the point (k, ω). For the dispersion relation depicted here, c_g is less than c.

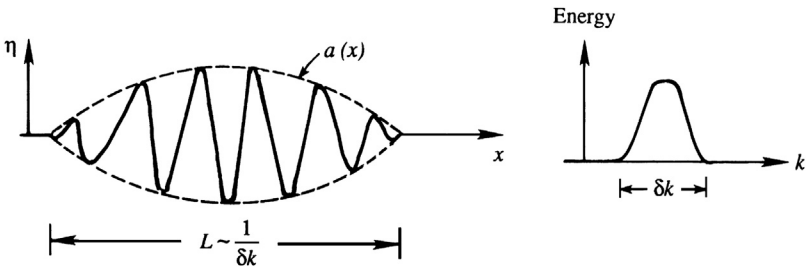

FIGURE 7.15 A wave packet composed of a wave number lying in a confined bandwidth δk. The length of the wave packet in physical space is proportional to $1/\delta k$. Thus, narrowband packets are longer than broadband packets.

that c_g is the speed of energy propagation is also evident in Figure 7.13 because the nodal points travel at c_g and no energy crosses nodal points.

For surface gravity waves having the dispersion relation (7.29), the group velocity is found to be

$$c_g = \frac{c}{2}\left[1 + \frac{2kH}{\sinh(2kH)}\right], \tag{7.69}$$

which has two limiting cases:

$$c_g = c/2\text{(deep water)}, \text{ and } c_g = c\text{(shallow water)}. \tag{7.70}$$

The group velocity of deep-water gravity waves is half the deep-water phase speed while shallow-water waves are nondispersive with $c = c_g$. For a linear nondispersive system, any waveform preserves its shape as it travels because all the wavelengths that make up the waveform travel at the same speed. For a pure capillary wave, the group velocity is $c_g = 3c/2$ (Exercise 7.9).

The rate of energy transmission for gravity waves is given by (7.44), namely

$$F = E\frac{c}{2}\left[1 + \frac{2kH}{\sinh(2kH)}\right] = Ec_g, \tag{7.71}$$

where $E = \rho g a^2/2$ is the average energy in the water column per unit horizontal area. This signifies that the *rate of transmission of energy of a sinusoidal wave component is wave energy times the group velocity,* and reinforces the interpretation of the group velocity as the speed of propagation of wave energy.

In three dimensions, the dispersion relation $\omega = \omega(k, l, m)$ may depend on all three components of the wave number vector $\mathbf{K} = (k, l, m)$. Here, using index notation, the group velocity vector is given by

$$c_{gi} = \frac{\partial \omega}{\partial K_i},$$

so the group velocity vector is the gradient of ω in the wave number space.

As mentioned in connection with (7.29) and (7.59), deep-water wave dispersion readily explains the evolution of the surface disturbance generated by dropping a stone into a quiescent pool, pond, or lake. Here, the initial disturbance can be thought of as being composed of a great many wavelengths, but the longer ones will travel faster. A short time after impact, at

$t = t_1$, the water surface may have the rather irregular profile shown in Figure 7.16. The appearance of the surface at a later time t_2, however, is more regular, with the longer components (which travel faster) out in front. The waves in front are the longest waves produced by the initial disturbance. Their length, $\lambda_{\max}$, is typically a few times larger than the dropped object. The leading edge of the wave system therefore propagates at the group speed of these wavelengths:

$$c_{\mathrm{g\ max}} = \frac{1}{2}\sqrt{\frac{g\lambda_{\mathrm{max}}}{2\pi}}.$$

Of course, pure capillary waves can propagate faster than this speed, but they may have small amplitudes and are dissipated quickly. Interestingly, the region of the impact becomes calm because there is a minimum group velocity of water waves due to the influence of surface tension, namely 17.8 cm/s (Exercise 7.10). The trailing edge of the wave system therefore travels at speed

$$c_{\mathrm{g\ min}} = 17.8\ \mathrm{cm/s}.$$

With $c_{\mathrm{gmax}} > 17.8$ cm/s for ordinary hand-size stones, the length of the disturbed region gets larger, as shown in Figure 7.16. The wave heights become correspondingly smaller because there is a fixed amount of energy in the wave system. (Wave dispersion, therefore, makes the linearity assumptions more accurate.) The smoothing of the waveform and the spreading of the region of disturbance continue until the amplitudes become imperceptible or the waves are damped by viscous dissipation (Exercise 7.11). It is clear that the *initial superposition of various wavelengths, running for some time, will sort themselves from slowest to fastest traveling components* since the different sinusoidal components, differing widely in their wave numbers, become spatially *separated*, with the slow ones close to the point of impact and

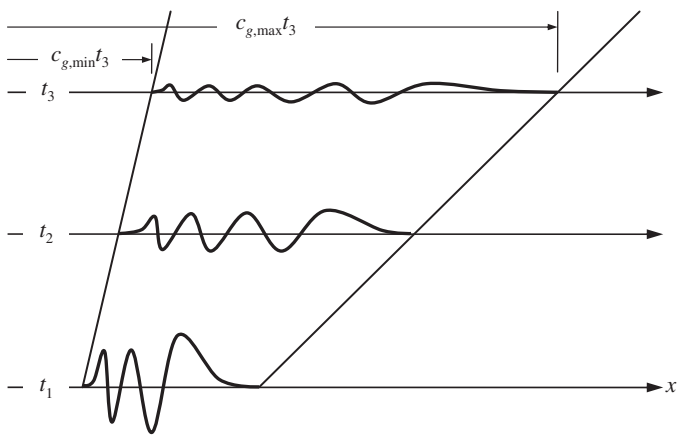

FIGURE 7.16 Generic surface profiles at three successive times of the wave train produced by dropping a stone into a deep quiescent pool. As time increases, the initial disturbance's long-wave (low-frequency) components travel faster than its short-wave (high-frequency) components. Thus, the wave train lengthens, the number of crests and troughs increases, and amplitudes fall (to conserve energy).

the fast ones further away. This is a basic feature of the behavior of dispersive wave propagation.

In the case of deep-water surface waves described here, the wave group as a whole travels slower than individual crests. Therefore, if we try to follow the last crest at the rear of the train, quite soon it is the second one from the rear; a new crest has appeared behind it. In fact, new crests are constantly appearing at the rear of the train, propagating through the train, and finally disappearing at the front of the train. This is because, by following a particular crest, we are traveling at roughly twice the speed at which the wave energy is traveling. Consequently, *we do not see a wave of fixed wavelength if we follow a particular crest*. In fact, an individual wave constantly becomes longer as it propagates through the train. When its length becomes equal to the longest wave generated initially, it cannot evolve anymore and dies out. Clearly, the waves at the front of the train are the longest Fourier components present in the initial disturbance. In addition, the temporal frequencies of the highest and lowest speed wave components of the wave group are typically different enough so that the number of wave crests in the train increases with time.

Another way to understand the group velocity is to consider the k or λ determined by an observer traveling at speed c_g with a slowly varying wave train described by

$$\eta = a(x,t)\cos[\theta(x,t)], \tag{7.72}$$

in an otherwise quiescent pool of water with constant depth H. Here $a(x, t)$ is a slowly varying amplitude and $\theta(x, t)$ is the local phase. For a specific wave number k and frequency ω, the phase is $\theta = kx - \omega t$. For a slowly varying wave train, define the *local* wave number $k(x, t)$ and the *local* frequency $\omega(x, t)$ as the rate of change of phase in space and time, respectively,

$$k(x,t) \equiv (\partial/\partial x)\theta(x,t) \text{ and } \omega(x,t) \equiv -(\partial/\partial t)\theta(x,t). \tag{7.73}$$

Cross differentiation leads to

$$\partial k/\partial t + \partial\omega/\partial x = 0, \tag{7.74}$$

but when there is a dispersion relationship $\omega = \omega(k)$, the spatial derivative of ω can be rewritten using the chain rule, $\partial\omega/\partial x = (d\omega/dk)\partial k/\partial x$, so that (7.74) becomes

$$\frac{\partial k}{\partial t} + c_g\frac{\partial k}{\partial x} = 0, \tag{7.75}$$

where $c_g = d\omega/dk$. The left-hand side of (7.75) is similar to the material derivative and gives the rate of change of k as seen by an observer traveling at speed c_g, which in this case is zero. Therefore, such an observer will always see the same wavelength. The *group velocity is therefore the speed at which wave numbers are advected*. This is shown in the xt-diagram of Figure 7.17, where wave crests follow lines with $dx/dt = c$ and wavelengths are preserved along the lines $dx/dt = c_g$. Note that the width of the disturbed region, bounded by the first and last thick lines in Figure 7.17, increases with time, and that the crests constantly appear at the back of the group and vanish at the front.

Now consider the same traveling observer, but allow there to be smooth variations in the water depth $H(x)$. Such depth variation creates an inhomogeneous medium when the waves are long enough to feel the presence of the bottom. Here, the dispersion relationship will be

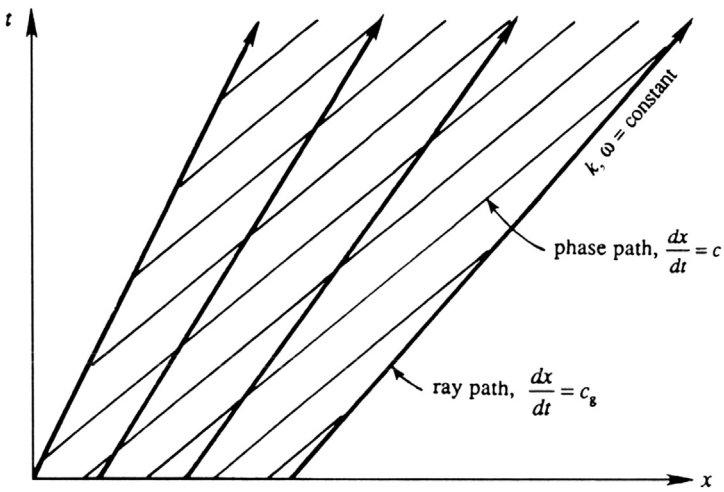

FIGURE 7.17 Propagation of a wave group in a homogeneous medium, represented on an x-t plot. Thin lines indicate paths taken by wave crests, and thick lines represent paths along which k and ω are constant. *M. J. Lighthill,* Waves in Fluids, *1978, reprinted with the permission of Cambridge University Press, London.*

$$\omega = \sqrt{gk \tanh [kH(x)]},$$

which is of the form

$$\omega = \omega(k, x). \tag{7.76}$$

Thus, a local value of the group velocity can be defined:

$$\partial\omega(k, x)/\partial k = c_g, \tag{7.77}$$

which on multiplication by $\partial k/\partial t$ gives

$$c_g \frac{\partial k}{\partial t} = \frac{\partial \omega}{\partial k}\frac{\partial k}{\partial t} = \frac{\partial \omega}{\partial t}. \tag{7.78}$$

Multiplying (7.74) by c_g and using (7.78) we obtain

$$\frac{\partial \omega}{\partial t} + c_g \frac{\partial \omega}{\partial x} = 0. \tag{7.79}$$

In three dimensions, this implies

$$\partial\omega/\partial t + \mathbf{c}_g \cdot \nabla\omega = 0,$$

which shows that ω, the frequency of the wave, remains constant to an observer traveling with the group velocity in an inhomogeneous medium.

Summarizing, an observer traveling at c_g in a homogeneous medium sees constant values of k, $\omega(k)$, c, and $c_g(k)$. Consequently, ray paths describing group velocity in the x-t plane are straight lines (Figure 7.17). In an inhomogeneous medium ω remains constant along the lines $dx/dt = c_g$, but k, c, and c_g can change. Consequently, ray paths are not straight in this case (Figure 7.18).

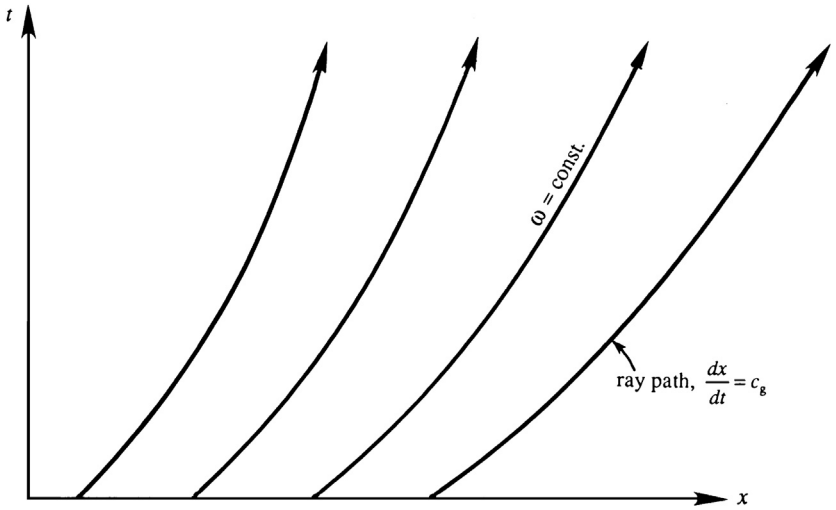

FIGURE 7.18 Propagation of a wave group in an inhomogeneous medium represented on an *x-t* plot. Only ray paths along which ω is constant are shown. *M. J. Lighthill,* Waves in Fluids, *1978, reprinted with the permission of Cambridge University Press, London.*

7.6. NONLINEAR WAVES IN SHALLOW AND DEEP WATER

In the first five sections of this chapter, the wave slope has been assumed to be small enough so that neglect of higher-order terms in the Bernoulli equation and application of the boundary conditions at $z = 0$ instead of at the free surface $z = \eta$ are acceptable approximations. One consequence of such linear analysis has been that shallow-water waves of arbitrary shape propagate unchanged in form. The unchanging form results from the fact that all wavelengths composing the initial waveform propagate at the same speed, $c = (gH)^{1/2}$, provided all the sinusoidal components satisfy the shallow-water approximation $kH \ll 1$. Such waveform invariance no longer occurs if *finite amplitude* effects are considered. This and several other nonlinear effects will also be discussed in this section.

Finite amplitude effects can be formally treated by the *method of characteristics*; this is discussed, for example, in Liepmann and Roshko (1957) and Lighthill (1978). Instead, a qualitative approach is adopted here. Consider a finite amplitude surface displacement consisting of a wave crest and trough, propagating in shallow-water of undisturbed depth H (Figure 7.19). Let a little wavelet be superposed on the crest at point x', at which the water depth is H' and the fluid velocity due to the wave motion is $u(x')$. Relative to an observer moving with the fluid velocity u, the wavelet propagates at the local shallow-water speed $c' = \sqrt{gH'}$. The speed of the wavelet relative to a frame of reference fixed in the undisturbed fluid is therefore $c = c' + u$. It is apparent that the local wave speed c is no longer constant because $c'(x)$ and $u(x)$ are variables. This is in contrast to the linearized theory in which u is negligible and c' is constant because $H' \approx H$.

Let us now examine the effect of variable phase speed on the wave profile. The value of c' is larger for points near the wave crest than for points in the wave trough. From Figure 7.5 we

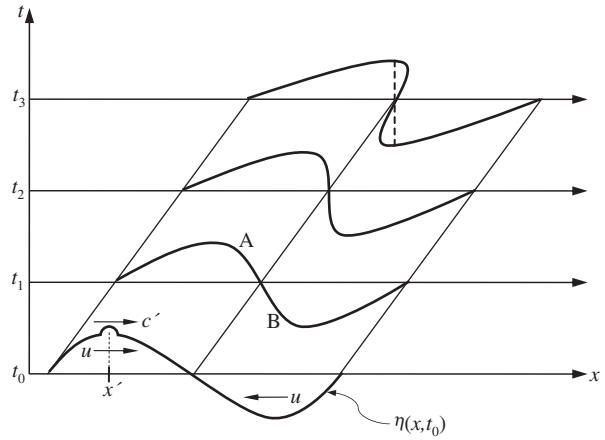

FIGURE 7.19 Finite-amplitude surface wave profiles at four successive times. When the wave amplitude is large enough, the fluid velocity below a crest or trough may be an appreciable fraction of the phase speed. This will cause wave crests to overtake wave troughs and will steepen the compressive portion of the wave (section A-B at time t_1). As this steepening continues, the wave-compression surface slope may become very large (t_2), or the wave may overturn and become a plunging breaker (t_3). Depending on the dynamics of the actual wave, the conditions shown at t_2 and t_3 may or may not occur since additional nonlinear processes (not described here) may contribute to the wave's evolution after t_1. If the waves were longitudinal (as in one-dimensional gas dynamics), the waveform at t_2 would represent a nascent shockwave, while the waveform at t_3 would represent a fully formed shockwave and would follow the dashed line to produce a single-valued profile.

also know that the fluid velocity u is positive (i.e., in the direction of wave propagation) under a wave crest and negative under a trough. It follows that wave speed c is larger for points on the crest than for points on the trough, so that the waveform deforms as it propagates, the crest region tending to overtake the trough region (Figure 7.19).

We shall call the front face AB a *compression region* because the surface here is rising with time and this implies an increase in pressure at any depth within the liquid. Figure 7.19 shows that the net effect of nonlinearity is a steepening of the compression region. For finite amplitude waves in a nondispersive medium like shallow water, therefore, there is an important distinction between compression and expansion regions. A compression region tends to steepen with time, while an expansion region tends to flatten out. This eventually would lead to the wave shape shown at the top of Figure 7.19, where there are three values of surface elevation at a point. While this situation is certainly possible and is readily observed as plunging breakers develop in the surf zone along ocean coastlines, the actual wave dynamics of such a situation lie beyond the scope of this discussion. However, even before the formation of a plunging breaker, the wave slope becomes infinite (profile at t_2 in Figure 7.19), so that additional physical processes including wave breaking, air entrainment, and foaming become important, and the current ideal flow analysis becomes inapplicable. Once the wave has broken, it takes the form of a front that propagates into still fluid at a constant speed that lies between $\sqrt{gH_1}$ and $\sqrt{gH_2}$, where H_1 and H_2 are the water depths on the two sides of the front (Figure 7.20). Such a wave is called a *hydraulic jump*, and it is similar to a *shockwave* in a compressible flow. Here it should be noted that the t_3 wave profile shown in Figure 7.19 is

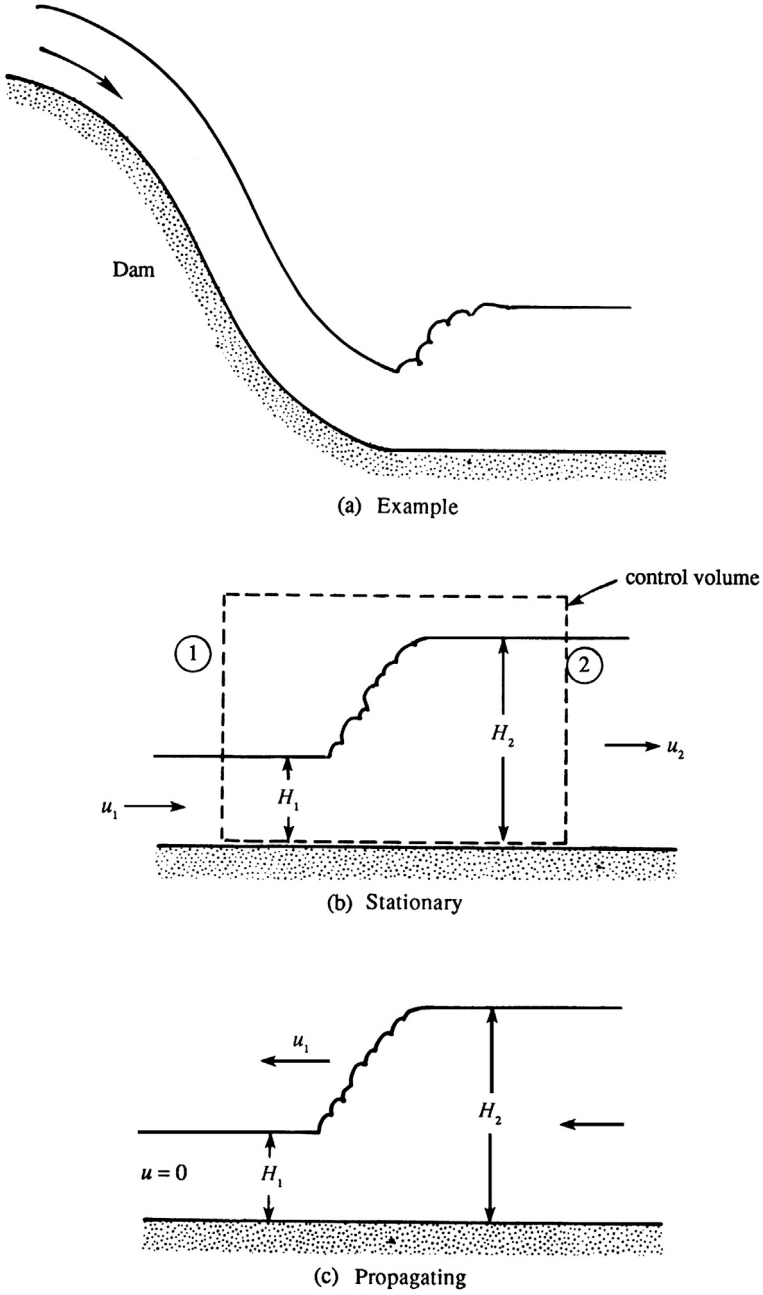

FIGURE 7.20 Schematic cross-section drawings of hydraulic jumps. (a) A stationary hydraulic jump formed at the bottom of a damn's spillway. (b) A stationary hydraulic jump and a stationary rectangular control volume with vertical inlet surface (1) and vertical outlet surface (2). (c) A hydraulic jump moving into a quiescent fluid layer of depth H_1. The flow speed behind the jump is nonzero.

not possible for longitudinal gas-dynamic compression waves. Such a profile instead leads to a shockwave with a front shown by the dashed line.

To analyze a hydraulic jump, consider the flow in a shallow canal of depth H. If the flow speed is u, we may define a dimensionless speed via the Froude number, Fr:

$$\mathrm{Fr} \equiv u/\sqrt{gH} = u/c. \tag{4.104}$$

The Froude number is analogous to the *Mach number* in compressible flow. The flow is called *supercritical* if $\mathrm{Fr} > 1$, and *subcritical* if $\mathrm{Fr} < 1$. For the situation shown in Figure 7.20b, where the jump is stationary, the upstream flow is supercritical while the downstream flow is subcritical, just as a compressible flow changes from supersonic to subsonic by going through a shockwave (see Chapter 15). The depth of flow is greater downstream of a hydraulic jump, just as the gas pressure is greater downstream of a shockwave. However, dissipative processes act within shockwaves and hydraulic jumps so that mechanical energy is lost in both cases. An example of a stationary hydraulic jump is found at the foot of a dam, where the flow almost always reaches a supercritical state because of the freefall (Figure 7.20a). A tidal bore propagating into a river mouth is an example of a propagating hydraulic jump. A circular hydraulic jump can be made by directing a vertically falling water stream onto a flat horizontal surface (Exercise 4.22).

The planar hydraulic jump shown in cross section in Figure 7.20b can be analyzed by using the dashed control volume shown, the goal being to determine how the depth ratio depends on the upstream Froude number. As shown, the depth rises from H_1 to H_2 and the velocity falls from u_1 to u_2. If the velocities are uniform through the depth and Q is the volume flow rate per unit width normal to the plane of the paper, then mass conservation requires

$$Q = u_1 H_1 = u_2 H_2.$$

Conserving momentum with the same control volume via (4.17) with $d/dt = 0$ and $\mathbf{b} = 0$ produces

$$\rho Q(u_2 - u_1) = \frac{1}{2}\rho g\left(H_1^2 - H_2^2\right),$$

where the left-hand terms come from the outlet and inlet momentum fluxes, and the right-hand terms are the hydrostatic pressure forces. Substituting $u_1 = Q/H_1$ and $u_2 = Q/H_2$ on the right side yields:

$$Q^2\left(\frac{1}{H_2} - \frac{1}{H_1}\right) = \frac{1}{2}g\left(H_1^2 - H_2^2\right). \tag{7.80}$$

After canceling out a common factor of $H_1 - H_2$, this can be rearranged to find:

$$\left(\frac{H_2}{H_1}\right)^2 + \frac{H_2}{H_1} - 2\mathrm{Fr}_1^2 = 0,$$

where $\mathrm{Fr}_1^2 = Q^2/gH_1^3 = u_1^2/gH_1$. The physically meaningful solution is

$$\frac{H_2}{H_1} = \frac{1}{2}\left(-1 + \sqrt{1 + 8\mathrm{Fr}_1^2}\right). \tag{7.81}$$

For supercritical flows $\mathrm{Fr}_1 > 1$, for which (7.81) shows that $H_2 > H_1$, and this verifies that water depth increases through a hydraulic jump.

Although a solution with $H_2 < H_1$ for $\mathrm{Fr}_1 < 1$ is mathematically allowed, such a solution violates the second law of thermodynamics, because it implies an increase of mechanical energy through the jump. To see this, consider the mechanical energy of a fluid particle at the surface, $E = u^2/2 + gH = Q^2/2H^2 + gH$. Eliminating Q by using (7.80) we obtain, after some algebra,

$$E_2 - E_1 = -(H_2 - H_1)\frac{g(H_2 - H_1)^2}{4H_1H_2}.$$

This shows that $H_2 < H_1$ implies $E_2 > E_1$, which violates the second law of thermodynamics. The mechanical energy, in fact, *decreases* in a hydraulic jump because of the action of viscosity.

Hydraulic jumps are not limited to air-water interfaces and may also appear at density interfaces in a stratified fluid, in the laboratory as well as in the atmosphere and the ocean. (For example, see Turner, 1973, Figure 3.11, for a photograph of an internal hydraulic jump on the lee side of a mountain.)

In a nondispersive medium, nonlinear effects may continually accumulate until they become large changes. Such an accumulation is prevented in a dispersive medium because the different Fourier components propagate at different speeds and tend to separate from each other. In a dispersive system, then, nonlinear steepening could cancel out the dispersive spreading, resulting in finite amplitude waves of constant form. This is indeed the case. A brief description of the phenomenon is given here; further discussion can be found in Whitham (1974), Lighthill (1978), and LeBlond and Mysak (1978).

In 1847 Stokes showed that periodic waves of finite amplitude are possible in deep water. In terms of a power series in the amplitude a, he showed that the surface deflection of irrotational waves in deep water is given by

$$\eta = a\cos k(x - ct) + \frac{1}{2}ka^2\cos 2k(x - ct) + \frac{3}{8}k^2a^3\cos 3k(x - ct) + \ldots, \tag{7.82}$$

where the speed of propagation is

$$c = \sqrt{\frac{g}{k}\left(1 + k^2a^2 + \ldots\right)}. \tag{7.83}$$

Equation (7.82) shows the first three terms in a Fourier series for the waveform η. The addition of Fourier components of different wavelengths in (7.82) shows that the wave profile η is no longer exactly sinusoidal. The arguments in the cosine terms show that all the Fourier components propagate at the same speed c, so that the wave profile propagates unchanged in time. It has now been established that the existence of periodic wave trains of unchanging form is a typical feature of nonlinear dispersive systems. Another important result, generally valid for nonlinear systems, is that the wave speed depends on the amplitude, as in (7.83).

Periodic finite-amplitude irrotational waves in deep water are frequently called *Stokes waves*. They have a flattened trough and a peaked crest (Figure 7.21). The maximum possible amplitude is $a_{\max} = 0.07\lambda$, at which point the crest becomes a sharp 120° angle. Attempts at generating waves of larger amplitude result in the appearance of foam (*white caps*) at these sharp crests.

FIGURE 7.21 The waveform of a Stokes wave. Stokes waves are finite-amplitude, periodic irrotational waves in deep water with crests that are more pointed and troughs that are broader than sinusoidal waves.

When finite amplitude waves are present, fluid particles no longer trace closed orbits, but undergo a slow drift in the direction of wave propagation. This is called *Stokes drift*. It is a second-order or finite-amplitude effect that causes fluid particle orbits to no longer close and instead take a shape like that shown in Figure 7.22. The mean velocity of a fluid particle is therefore not zero, although the mean velocity at a fixed point in space must be zero if the wave motion is periodic. The drift occurs because the particle moves forward faster when at the top of its trajectory than it does backward when at the bottom of its trajectory.

To find an expression for the Stokes drift, start from the path-line equations (7.32) for the fluid particle trajectory $\mathbf{x}_p(t) = x_p(t)\mathbf{e}_x + z_p(t)\mathbf{e}_z$, but this time include first-order variations in the u and w fluid velocities via a first-order Taylor series in $\xi = x_p - x_0$, and $\zeta = z_p - z_0$:

$$\frac{dx_p(t)}{dt} = u(x_p, z_p, t) = u(x_0, z_0, t) + \xi\left(\frac{\partial u}{\partial x}\right)_{x_0, z_0} + \zeta\left(\frac{\partial u}{\partial z}\right)_{x_0, z_0} + \ldots, \tag{7.84a}$$

and

$$\frac{dz_p(t)}{dt} = w(x_p, z_p, t) = w(x_0, z_0, t) + \xi\left(\frac{\partial w}{\partial x}\right)_{x_0, z_0} + \zeta\left(\frac{\partial w}{\partial z}\right)_{x_0, z_0} + \ldots, \tag{7.84b}$$

where (x_0, z_0) is the fluid element location in the absence of wave motion. The Stokes drift is the time average of (7.84a). However, the time average of $u(x_0, z_0, t)$ is zero; thus, the Stokes drift is given by the time average of the next two terms of (7.84a). These terms were neglected in the fluid particle trajectory analysis in Section 7.2, and the result was closed orbits.

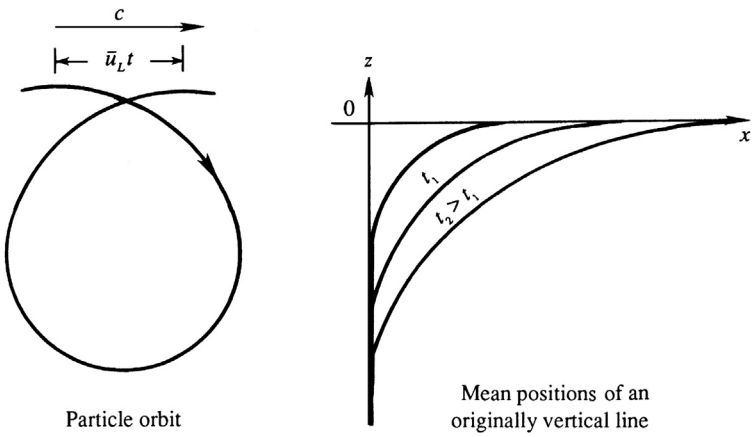

FIGURE 7.22 The Stokes drift. The drift velocity $\bar{u}_L$ is a finite-amplitude effect and occurs because near-surface fluid particle paths are no longer closed orbits. The mean position of an initially vertical line of fluid particles extending downward from the liquid surface will increasingly bend in the direction of wave propagation with increasing time.

For deep-water gravity waves, the Stokes drift speed $\overline{u}_L$ can be estimated by evaluating the time average of (7.84a) using (7.46) and (7.47) to produce:

$$\overline{u}_L = a^2 \omega k e^{2kz_0}, \tag{7.85}$$

which is the Stokes drift speed in deep water. Its surface value is $a^2\omega k$, and the vertical decay rate is twice that for the fluid velocity components. It is therefore confined very close to the sea surface. For arbitrary water depth, (7.85) may be generalized to

$$\overline{u}_L = a^2 \omega k \frac{\cosh(2k(z_0 + H))}{2\sinh^2(kH)} \tag{7.86}$$

(Exercise 7.14). As might be expected, the vertical component of the Stokes drift is zero.

The Stokes drift causes mass transport in the fluid so it is also called the *mass transport velocity*. A vertical column of fluid elements marked by some dye gradually bends near the surface (Figure 7.22). In spite of this mass transport, the mean fluid velocity at any point that resides within the liquid for the entire wave period is exactly zero (to any order of accuracy), if the flow is irrotational. This follows from the condition of irrotationality $\partial u/\partial z = \partial w/\partial x$, a vertical integral which gives

$$u = u|_{z=-H} + \int_{-H}^{z} \frac{\partial w}{\partial x} dz,$$

showing that the mean of u is proportional to the mean of $\partial w/\partial x$ over a wavelength, which is zero for periodic flows.

There are also a variety of wave analyses for specialized circumstances that involve dispersion, nonlinearity, and viscosity to varying degrees. So, before moving on to internal waves, one of the classical examples of this type of specialization is presented here for nonlinear waves that are slightly dispersive. In 1895 Korteweg and de Vries showed that waves with λ/H in the range between 10 and 20 satisfy:

$$\frac{\partial \eta}{\partial t} + c_0 \frac{\partial \eta}{\partial x} + \frac{3}{2} c_0 \frac{\eta}{H} \frac{\partial \eta}{\partial x} + \frac{1}{6} c_0 H^2 \frac{\partial^3 \eta}{\partial x^3} = 0, \tag{7.87}$$

where $c_0 = \sqrt{gH}$. This is the *Korteweg–de Vries equation*. The first two terms are linear and nondispersive. The third term is nonlinear and represents finite amplitude effects. The fourth term is linear and results from weak dispersion due to the water depth not being shallow enough. If the nonlinear term in (7.87) is neglected, then setting $\eta = a\cos(kx - \omega t)$ leads to the dispersion relation $c = c_0\,(1 - (1/6)k^2H^2)$. This agrees with the first two terms in the Taylor series expansion of the dispersion relation $c = \sqrt{(g/k)\tanh kH}$ for small kH, verifying that weak dispersive effects are indeed properly accounted for by the last term in (7.87).

The ratio of nonlinear and dispersion terms in (7.88) is

$$\frac{\eta\,\partial\eta}{H\partial x} \Big/ H^2 \frac{\partial^3 \eta}{\partial x^3} \sim \frac{a\lambda^2}{H^3}.$$

When $a\lambda^2/H^3$ is larger than ~16, nonlinear effects sharpen the forward face of the wave, leading to a hydraulic jump, as discussed earlier in this section. For lower values of

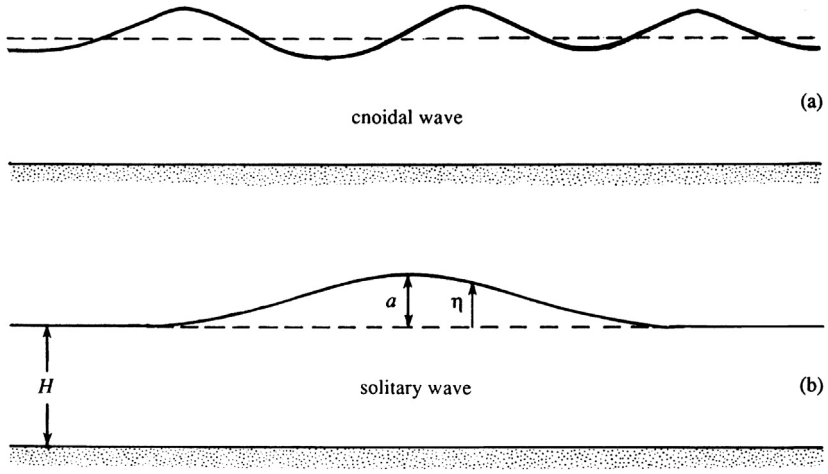

FIGURE 7.23 Finite-amplitude waves of unchanging form: (a) cnoidal waves and (b) a solitary wave. In both cases, the processes of nonlinear steepening and dispersive spreading balance so that the waveform is unchanged.

$a\lambda^2/H^3$, a balance can be achieved between nonlinear steepening and dispersive spreading, and waves of unchanging form become possible.

Analysis of the Korteweg–de Vries equation shows that two types of solutions are then possible—a periodic solution and a solitary wave solution. The periodic solution is called a *cnoidal wave*, because it is expressed in terms of elliptic functions denoted by $cn(x)$. Its waveform is shown in Figure 7.23. The other possible solution of the Korteweg–de Vries equation involves only a single wave crest and is called a *solitary wave* or *soliton*. Its profile is given by

$$\eta = a\,\mathrm{sech}^2\left[\left(\frac{3a}{4H^3}\right)^{1/2}(x-ct)\right], \tag{7.88}$$

where the speed of propagation is

$$c = c_0\left(1+\frac{a}{2H}\right),$$

showing that the propagation velocity increases with amplitude. The validity of (7.88) can be checked by substitution into (7.87) (Exercise 7.15). The waveform of the solitary wave is shown in Figure 7.23.

An isolated hump propagating at constant speed with unchanging form and in fairly shallow water was first observed experimentally by S. Russell in 1844. Solitons have been observed to exist not only as surface waves, but also as internal waves in stratified fluids, in the laboratory as well as in the ocean (see Turner, 1973, Figure 3.3).

7.7. WAVES ON A DENSITY INTERFACE

To this point, waves at the surface of a liquid have been considered without regard to the gas (or liquid) above the surface. Yet, gravity and capillary waves can also exist at the

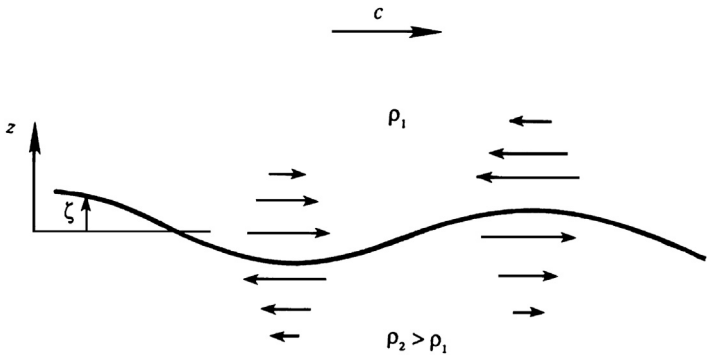

FIGURE 7.24 Internal wave at a density interface between two infinitely deep fluids. Here the horizontal velocity is equal and opposite above and below the interface, so there is a time-dependent vortex sheet at the interface.

interface between two immiscible liquids of different densities. A sharp-density gradient can be readily generated in the laboratory (at least temporarily) between gases with different densities, and between oil and water. In the ocean sharp-density gradients may be generated by solar heating of the upper layer, or in an estuary (that is, a river mouth) or a fjord into which fresh (less saline) river water flows over oceanic water, which is more saline and consequently heavier. The basic situation can be idealized by considering a lighter fluid of density ρ_1 lying over a heavier fluid of density ρ_2 (Figure 7.24).

For simplicity ignore interfacial (surface) tension, and assume that only small-slope linear waves exist on the interface and that both fluids are infinitely deep, so that only those solutions that decay exponentially from the interface are allowed. In this section and in the rest of this chapter, *complex notation* will be used to ease the algebraic and trigonometric effort. This means that (7.2) will be replaced by

$$\zeta(x,t) = \mathrm{Re}\{a\exp[i(kx-\omega t)]\},$$

where Re{} is the operator that extracts the real part of the complex function in {}-braces, and $i=\sqrt{-1}$ as usual. When using complex numbers and variables in linear mathematical analyses it is customary to drop Re{} and simply write

$$\zeta(x,t) = a\exp[i(kx-\omega t)] \tag{7.89}$$

until reporting the final results when Re{} commonly reappears. Any analysis done with (7.89) includes an imaginary part, sometimes denoted Im{}, that winds up being of no consequence in the final results.

To determine wave properties in this situation, the Laplace equation for the velocity potential must be solved in both fluids subject to the continuity of p and w at the interface. The equations are

$$\frac{\partial^2\phi_1}{\partial x^2}+\frac{\partial^2\phi_1}{\partial z^2}=0 \quad \text{and} \quad \frac{\partial^2\phi_2}{\partial x^2}+\frac{\partial^2\phi_2}{\partial z^2}=0, \tag{7.90}$$

subject to

$$\phi_1 \to 0 \quad \text{as} \quad z\to\infty, \tag{7.91}$$

$$\phi_2 \to 0 \quad \text{as} \quad z\to -\infty, \tag{7.92}$$

$$\frac{\partial \phi_1}{\partial z} = \frac{\partial \phi_2}{\partial z} = \frac{\partial \zeta}{\partial t} \quad \text{at } z = 0, \text{ and} \tag{7.93}$$

$$\rho_1 \frac{\partial \phi_1}{\partial t} + \rho_1 g\zeta = \rho_2 \frac{\partial \phi_2}{\partial t} + \rho_2 g\zeta \quad \text{at } z = 0. \tag{7.94}$$

Equation (7.93) follows from equating the vertical velocity of the fluid on both sides of the interface to the rate of rise of the interface. Equation (7.94) follows from the continuity of pressure across the interface in the absence of interfacial (surface) tension, $\sigma = 0$. As in the case of surface waves, the boundary conditions are linearized and applied at $z = 0$ instead of at $z = \zeta$. Conditions (7.91) and (7.92) require that the solutions of (7.90) must be of the form

$$\phi_1 = A\, e^{-kz} e^{i(kx-\omega t)} \text{ and}$$
$$\phi_2 = B\, e^{kz} e^{i(kx-\omega t)},$$

because a solution proportional to e^{kz} is not allowed in the upper fluid, and a solution proportional to e^{-kz} is not allowed in the lower fluid. Here the amplitudes A and B can be complex. As in Section 7.2, the constants are determined from the kinematic boundary conditions (7.93), giving

$$A = -B = i\omega a/k.$$

The dynamic boundary condition (7.94) then leads to the dispersion relation

$$\omega = \sqrt{gk\left(\frac{\rho_2 - \rho_1}{\rho_2 + \rho_1}\right)} = \varepsilon\sqrt{gk}, \tag{7.95}$$

where $\varepsilon^2 \equiv (\rho_2 - \rho_1)/(\rho_2 + \rho_1)$ is a small number if the density difference between the two liquids is small. The case of small density difference is relevant in geophysical situations; for example, a 10°C temperature change causes the density of an upper layer of the ocean to decrease by 0.3%. Equation (7.95) shows that waves at the interface between two liquids of infinite thickness travel like deep-water surface waves, with ω proportional to $\sqrt{gk}$, but at a frequency that is lower by the factor ε. In general, *internal waves have a lower frequency and slower phase speed than surface waves with the same wave number.* As expected, (7.95) recovers (7.45) as $\varepsilon \to 1$ when $\rho_1/\rho_2 \to 0$.

The kinetic energy E_k per unit area of interface of the field can be found by integrating $\rho(u^2 + w^2)/2$ over the range $z = \pm\infty$ (Exercise 7.16):

$$E_k = \frac{1}{4}(\rho_2 - \rho_1) g a^2.$$

The potential energy can be calculated by finding the work done in deforming a flat interface to the wave shape. In Figure 7.25, this involves a transfer of column A of density ρ_2 to location B, a simultaneous transfer of column B of density ρ_1 to location A, and integrating the work over *half the wavelength*, since the resulting exchange forms a complete wavelength; see the previous discussion of Figure 7.6. The potential energy per unit horizontal area is therefore

$$E_p = \frac{1}{\lambda}\int_0^{\lambda/2} \rho_2 g\zeta^2\, dx - \frac{1}{\lambda}\int_0^{\lambda/2} \rho_1 g\zeta^2\, dx = \frac{g(\rho_2 - \rho_1)}{2\lambda}\int_0^{\lambda/2} \zeta^2\, dx = \frac{1}{4}(\rho_2 - \rho_1) g a^2.$$

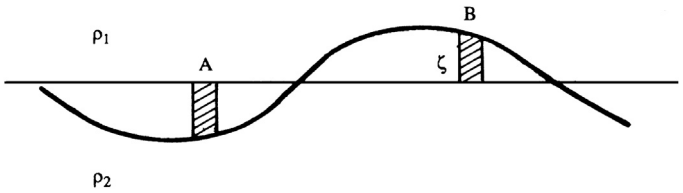

FIGURE 7.25 Geometry for calculating the potential energy of a sinusoidal displacement of the interface between two incompressible fluids with different densities. The work done in transferring element A to the vertical location of element B equals the weight of A times the vertical displacement of its center of gravity.

The total wave energy per unit horizontal area is

$$E = E_k + E_p = \frac{1}{2}(\rho_2 - \rho_1)ga^2. \tag{7.96}$$

In a comparison with (7.42), it follows that the amplitude of ocean internal waves is usually much larger than those of surface waves for the same amount of energy per unit interface area when $(\rho_2 - \rho_1) \ll \rho_2$.

The horizontal velocity components in the two layers are

$$u_1 = \frac{\partial \phi_1}{\partial x} = -\omega a e^{-kz} e^{i(kx-\omega t)} \text{ and}$$

$$u_2 = \frac{\partial \phi_2}{\partial x} = \omega a e^{kz} e^{i(kx-\omega t)},$$

and are oppositely directed (Figure 7.24). The interface is therefore a time-dependent *vortex sheet* and the tangential velocity is discontinuous across it. It can be expected that a continuously stratified medium, in which the density varies continuously as a function of z, will support internal waves whose vorticity is distributed throughout the flow. Consequently, *internal waves in a continuously stratified fluid are not irrotational and do not satisfy the Laplace equation*.

The existence of internal waves at a density discontinuity has explained an interesting phenomenon observed in Norwegian fjords (Gill, 1982). It was known for a long time that ships experienced unusually high drags on entering these fjords. The phenomenon was a mystery (and was attributed to "dead water") until Bjerknes, a Norwegian oceanographer, explained it as due to the internal waves at the interface generated by the motion of the ship (Figure 7.26). (Note that the product of the drag times the speed of the ship gives the rate of generation of wave energy, with other sources of resistance neglected.)

As a second example of an internal wave at a density discontinuity, consider the case in which the upper layer is not infinitely thick but has a finite thickness; the lower layer is initially assumed to be infinitely thick. The case of two infinitely deep liquids, treated in the preceding section, is then a special case of the present situation. Whereas only waves at the interface were allowed in the preceding section, the presence of a free surface now allows surface waves to enter the problem. It is clear that the present configuration will allow two modes of oscillation where the free-surface and interface waves are in or out of phase.

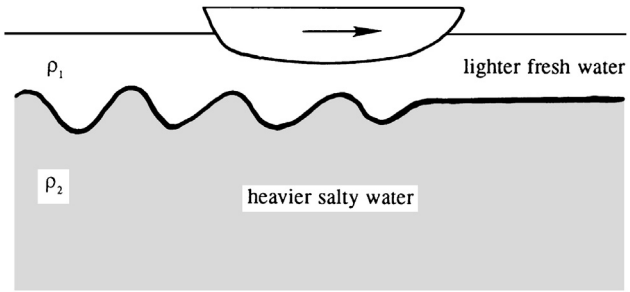

FIGURE 7.26 Schematic explanation for the phenomenon of *dead water* in Norwegian fjords. The ship on the ocean surface may produce waves on the ocean surface and on an interface between lighter, fresher water and cooler, saltier water. Wave production leads to drag on the ship and both types of waves are generated under certain conditions.

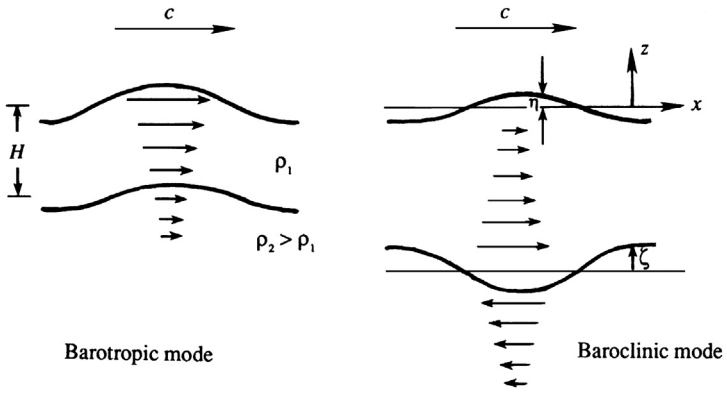

FIGURE 7.27 The two modes of motion of a layer of fluid overlying an infinitely deep fluid. The barotropic mode is an extension of the surface wave motion discussed in the first six sections of this chapter. The baroclinc mode is the extension of the interface wave motion described earlier in this section and shown in Figure 7.24. The baroclinic mode includes vorticity at the density interface; the barotropic mode does not.

To analyze this situation, let H be the thickness of the upper layer, and let the origin be placed at the mean position of the free surface (Figure 7.27). The field equations are (7.90) and the boundary conditions are:

$$\phi_2 \to 0 \quad \text{at } z \to -\infty, \tag{7.97}$$

$$\frac{\partial \phi_1}{dz} = \frac{\partial \eta}{\partial t} \quad \text{at } z = 0, \tag{7.98}$$

$$\frac{\partial \phi_1}{\partial t} + g\eta = 0 \quad \text{at } z = 0, \tag{7.99}$$

$$\frac{\partial \phi_1}{\partial z} = \frac{\partial \phi_2}{\partial z} = \frac{\partial \zeta}{\partial t} \quad \text{at } z = -H, \text{ and} \tag{7.100}$$

$$\rho_1 \frac{\partial \phi_1}{\partial t} + \rho_1 g\zeta = \rho_2 \frac{\partial \phi_2}{\partial t} + \rho_2 g\zeta \quad \text{at } z = -H. \tag{7.101}$$

In addition, assume a free-surface displacement of the form

$$\eta = ae^{i(kx-\omega t)}, \tag{7.102}$$

and an interface displacement of the form

$$\zeta = be^{i(kx-\omega t)}. \tag{7.103}$$

Without losing generality, we can regard a as real, which means that we are considering a surface wave of the form $\eta = a\cos(kx - \omega t)$. The constant b should be left complex since ζ and η may not be in phase, and the solution of the problem should determine such phase differences.

The velocity potentials in the layers must be of the form

$$\phi_1 = (A\, e^{kz} + B\, e^{-kz})\, e^{i(kx-\omega t)}, \tag{7.104}$$

$$\phi_2 = C\, e^{kz}\, e^{i(kx-\omega t)}. \tag{7.105}$$

The form (7.105) satisfies (7.97). Conditions (7.98) through (7.100) allow a solution for the constants in terms of a, ω, k, g, and H:

$$A = -\frac{ia}{2}\left(\frac{\omega}{k} + \frac{g}{\omega}\right), \tag{7.106}$$

$$B = \frac{ia}{2}\left(\frac{\omega}{k} - \frac{g}{\omega}\right), \tag{7.107}$$

$$C = -\frac{ia}{2}\left(\frac{\omega}{k} + \frac{g}{\omega}\right) - \frac{ia}{2}\left(\frac{\omega}{k} - \frac{g}{\omega}\right)e^{2kH}, \text{ and} \tag{7.108}$$

$$b = \frac{a}{2}\left(1 + \frac{gk}{\omega^2}\right)\, e^{-kH} + \frac{a}{2}\left(1 - \frac{gk}{\omega^2}\right)e^{kH}. \tag{7.109}$$

Substitution into (7.101) leads to the dispersion relation $\omega(k)$. After some algebraic manipulations, the result can be written as (see Exercise 7.19):

$$\left(\frac{\omega^2}{gk} - 1\right)\left\{\frac{\omega^2}{gk}[\rho_1 \sinh kH + \rho_2 \cosh kH] - (\rho_2 - \rho_1)\sinh kH\right\} = 0. \tag{7.110}$$

One possible root of (7.110) is

$$\omega^2 = gk, \tag{7.111}$$

which is the same as that for a deep-water gravity wave. Substituting (7.111) into (7.109) leads to

$$b = ae^{-kH}, \tag{7.112}$$

which implies that the interface waves are in phase with the surface waves but are reduced in amplitude by the factor e^{-kH}. This mode is similar to a gravity wave propagating on the free surface of the upper liquid, in which the motion decays as e^{-kz} from the free surface. It is called the *barotropic mode*, because the surfaces of constant pressure and density coincide.

The other root of (7.110) is

$$\omega^2 = \frac{gk(\rho_2 - \rho_1)\sinh kH}{\rho_2 \cosh kH + \rho_1 \sinh kH}, \tag{7.113}$$

which reduces to (7.95) when $kH \to \infty$. Substituting (7.113) into (7.109) leads to

$$\eta = -\zeta\left(\frac{\rho_2 - \rho_1}{\rho_1}\right)e^{-kH}, \tag{7.114}$$

which demonstrates that η and ζ have opposite signs and that the interface displacement (ζ) is much larger than the surface displacement (η) if the density difference is small. This is the *baroclinic* or *internal mode* because the surfaces of constant pressure and density do not coincide. Here the horizontal velocity u changes sign across the interface. The existence of a density difference has therefore generated a motion that is quite different from the barotropic mode, (7.111) and (7.112). The case described at the beginning of this section, where the fluids have infinite depth and no free surface, has only a baroclinic mode and no barotropic mode.

A very common simplification, frequently made in geophysical situations, involves assuming that the wavelengths are large compared to the upper layer depth. For example, the depth of the oceanic upper layer, below which there is a sharp-density gradient, could be ≈ 50 m thick, but interfacial waves much longer than this may be of interest. The relevant approximation in this case, $kH \ll 1$, is called the *shallow-water* or *long-wave approximation* and is implemented via:

$$\sinh(kH) \cong kH \quad \text{and} \quad \cosh(kH) \cong 1,$$

so the dispersion relation (7.113) corresponding to the baroclinic mode reduces to

$$\omega^2 = kg\left(\frac{\rho_2 - \rho_1}{\rho_2}\right)kH \tag{7.115}$$

to lowest order in the small parameter kH. The phase velocity of waves at the interface is

$$c = [g'H]^{1/2}, \quad \text{where } g' = g\left(\frac{\rho_2 - \rho_1}{\rho_2}\right) \tag{7.116, 7.117}$$

is the reduced gravity. Equation (7.116) is similar to the corresponding expression for *surface* waves in a shallow homogeneous layer of thickness H, namely, $c = \sqrt{gH}$, except that the speed is reduced by the factor $\sqrt{(\rho_2 - \rho_1)/\rho_2}$. This agrees with the previous conclusion that internal waves propagate slower than surface waves. Under the shallow-water approximation, (7.114) reduces to

$$\eta = -\zeta\left(\frac{\rho_2 - \rho_1}{\rho_1}\right). \tag{7.118}$$

In Section 7.2, the shallow-water approximation for surface waves is found equivalent to a hydrostatic approximation and results in a depth-independent horizontal velocity. This conclusion also holds for interfacial waves. The fact that u_1 is independent of z follows from (7.104) on noting that $e^{kz} \approx e^{-kz} \approx 1$. To see that pressure is hydrostatic, the perturbation pressure p' in the upper layer determined from (7.104) is

$$p\prime = -\rho_1\frac{\partial \phi_1}{\partial t} = i\rho_1\omega\,(A + B)\,e^{i(kx-\omega t)} = \rho_1 g\eta, \tag{7.119}$$

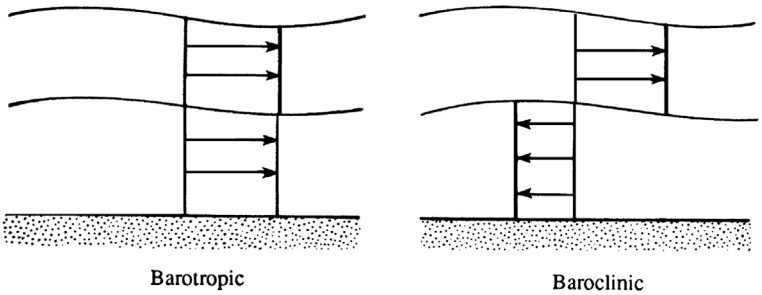

FIGURE 7.28 The two modes of motion in a shallow-water, two-layer system in the Boussinesq limit. These profiles are the limiting case of those in Figure 7.27 when the lower fluid layer depth is shallow. As before, the baroclinic mode includes vorticity at the density interface; the barotropic mode does not.

where the constants given in (7.106) and (7.107) have been used. This shows that p' is independent of z and equals the hydrostatic pressure change due to the free-surface displacement.

So far, the lower fluid has been assumed to be infinitely deep, resulting in an exponential decay of the flow field from the interface into the lower layer, with a decay scale of the order of the wavelength. If the lower layer is now considered thin compared to the wavelength, then the horizontal velocity will be depth independent, and the flow hydrostatic, in the lower layer. If *both* layers are considered thin compared to the wavelength, then the flow is hydrostatic (and the horizontal velocity field is depth independent) in *both* layers. This is the *shallow-water* or *long-wave approximation* for a two-layer fluid. In such a case the horizontal velocity field in the barotropic mode has a discontinuity at the interface, which vanishes in the Boussinesq limit $(\rho_2 - \rho_1)/\rho_1 \ll 1$. Under these conditions the two modes of a two-layer system have a simple structure (Figure 7.28): a barotropic mode in which the horizontal velocity is depth independent across the entire water column; and a baroclinic mode in which the horizontal velocity is directed in opposite directions in the two layers (but is depth independent in each layer).

7.8. INTERNAL WAVES IN A CONTINUOUSLY STRATIFIED FLUID

Waves may also exist in the interior of a pool, reservoir, lake, or ocean when the fluid's density in a quiescent state is a continuous function of the vertical coordinate z. The equations of motion for internal waves in such a stratified medium presented here are simplifications of the Boussinesq set specified at the end of Section 4.9. The Boussinesq approximation treats the density as constant, except in the vertical momentum equation. For simplicity, we shall also assume that: 1) the wave motion is effectively inviscid because the velocity gradients are small and the Reynolds number is large, 2) the wave amplitudes are small enough so that the nonlinear advection terms can be neglected, and 3) the frequency of wave motion is much larger than the Coriolis frequency so it does not affect the wave motion. Effects of the earth's rotation are considered in Chapter 13. The Boussinesq set then simplifies to:

$$\frac{D\rho}{Dt} = 0, \quad \frac{\partial u}{\partial x} + \frac{\partial v}{\partial y} + \frac{\partial w}{\partial z} = 0, \tag{4.9, 4.10}$$

$$\frac{\partial u}{\partial t} = -\frac{1}{\rho_0}\frac{\partial p}{\partial x}, \quad \frac{\partial v}{\partial t} = -\frac{1}{\rho_0}\frac{\partial p}{\partial y}, \quad \text{and} \quad \frac{\partial w}{\partial t} = -\frac{1}{\rho_0}\frac{\partial p}{\partial z} - \frac{\rho g}{\rho_0}, \tag{7.120, 7.121, 7.122}$$

where ρ_0 is a constant reference density. Here, (4.9) expresses constancy of fluid-particle density while (4.10) is the condition for incompressible flow. If temperature is the only agency that changes the density, then $D\rho/Dt = 0$ follows from the heat equation in the nondiffusive form $DT/Dt = 0$ and a temperature-only equation of state, in the form $\delta\rho/\rho = -\alpha\delta T$, where α is the coefficient of thermal expansion. If the density changes are due to changes in the concentration S of a constituent (e.g., salinity in the ocean or water vapor in the atmosphere), then $D\rho/Dt = 0$ follows from $DS/Dt = 0$ (the nondiffusive form of the constituent conservation equation) and a concentration-only equation of state, $\rho = \rho(S)$, in the form of $\delta\rho/\rho = \beta\delta S$, where β is the coefficient describing how the density changes due to concentration of the constituent. In both cases, the principle underlying $D\rho/Dt = 0$ is an equation of state that does not include pressure. In terms of common usage, this equation is frequently called the *density equation*, as opposed to the *continuity equation* (4.10).

The five equations (4.9), (4.10), and (7.120) through (7.122) contain five unknowns (u, v, w, p, ρ). Before considering wave motions, first define the quiescent density $\overline{\rho}(z)$ and pressure $\overline{p}(z)$ profiles in the medium as those that satisfy a hydrostatic balance:

$$0 = -\frac{1}{\rho_0}\frac{d\overline{p}}{dz} - \frac{\overline{\rho} g}{\rho_0}. \tag{7.123}$$

When the motion develops, the pressure and density will change relative to their quiescent values:

$$p = \overline{p}(z) + p', \quad \rho = \overline{\rho}(z) + \rho'. \tag{7.124}$$

The density equation (4.9) then becomes

$$\frac{\partial}{\partial t}(\overline{\rho} + \rho') + u\frac{\partial}{\partial x}(\overline{\rho} + \rho') + v\frac{\partial}{\partial y}(\overline{\rho} + \rho') + w\frac{\partial}{\partial z}(\overline{\rho} + \rho') = 0. \tag{7.125}$$

Here, $\partial\overline{\rho}/\partial t = \partial\overline{\rho}/\partial x = \partial\overline{\rho}/\partial y = 0$. The nonlinear terms (namely, $u\partial\rho'/\partial x$, $v\partial\rho'/\partial y$, and $w\partial\rho'/\partial z$) are also negligible for small-amplitude motions. The *linear* part of the fourth term, $w\, d\overline{\rho}/dz$, must be retained, so the linearized version of (4.9) is

$$\frac{\partial\rho'}{\partial t} + w\frac{d\overline{\rho}}{dz} = 0, \tag{7.126}$$

which states that the density perturbation at a point is generated only by the vertical advection of the *background* density distribution. We now introduce the *Brunt–Väisälä frequency*, or *buoyancy frequency*:

$$N^2 \equiv -\frac{g}{\rho_0}\frac{d\overline{\rho}}{dz}. \tag{7.127}$$

This is (1.29) when the adiabatic density gradient is zero. As described in Section 1.10, $N(z)$ has units of rad./s and is the oscillation frequency of a vertically displaced fluid particle released from rest in the absence of fluid friction. Using (7.123) and (7.127) in (7.120) through (7.122) and (7.126) produces

$$\frac{\partial u}{\partial t} = -\frac{1}{\rho_0}\frac{\partial p'}{\partial x}, \quad \frac{\partial v}{\partial t} = -\frac{1}{\rho_0}\frac{\partial p'}{\partial y}, \quad \frac{\partial w}{\partial t} = -\frac{1}{\rho_0}\frac{\partial p'}{\partial z} - \frac{\rho' g}{\rho_0}, \tag{7.128, 7.129, 7.130}$$

and

$$\frac{\partial \rho'}{\partial t} - \frac{N^2 \rho_0}{g} w = 0. \tag{7.131}$$

Comparing (7.120) through (7.122) and (7.128) through (7.130), we see that the only difference is the replacement of the total density ρ and pressure p with the perturbation density ρ' and pressure p'.

The full set of equations for linear wave motion in a stratified fluid are (4.10) and (7.128) through (7.131), where ρ may be a function of temperature T and concentration S of a constituent, but not of pressure. At first this does not seem to be a good assumption. The compressibility effects in the atmosphere are certainly not negligible; even in the ocean the density changes due to the huge changes in the background pressure are as much as 4%, which is ≈ 10 times the density changes due to the variations of the salinity and temperature. The effects of compressibility, however, can be handled within the Boussinesq approximation if we regard $\overline{\rho}$ in the definition of N as the background *potential density*, that is, the density distribution from which the adiabatic changes of density, due to the changes of pressure, have been subtracted out. The concept of potential density is explained in Chapter 1. Oceanographers account for compressibility effects by converting all their density measurements to the standard atmospheric pressure; thus, when they report variations in density (what they call "sigma tee") they are generally reporting variations due only to changes in temperature and salinity.

A useful condensation of the above equations involving only w can be obtained by taking the time derivative of (4.10) and using the horizontal momentum equations (7.128) and (7.129) to eliminate u and v. The result is

$$\frac{1}{\rho_0}\nabla_{\mathrm{H}}^2 p' = \frac{\partial^2 w}{\partial z\, \partial t}, \tag{7.132}$$

where $\nabla_{\mathrm{H}}^2 \equiv \partial^2/\partial x^2 + \partial^2/\partial y^2$ is the *horizontal* Laplacian operator. Elimination of ρ' from (7.130) and (7.131) gives

$$\frac{1}{\rho_0}\frac{\partial^2 p'}{\partial t\, \partial z} = -\frac{\partial^2 w}{\partial t^2} - N^2 w. \tag{7.133}$$

Finally, p' can be eliminated by taking ∇_{H}^2 (7.133), and inserting the result in (7.132) to find:

$$\frac{\partial^2}{\partial t\, \partial z}\left(\frac{\partial^2 w}{\partial t\, \partial z}\right) = -\nabla_{\mathrm{H}}^2\left(\frac{\partial^2 w}{\partial t^2} + N^2 w\right),$$

which can be written as

$$\frac{\partial^2}{\partial t^2}\nabla^2 w + N^2 \nabla_{\mathrm{H}}^2 w = 0, \tag{7.134}$$

where $\nabla^2 \equiv \partial^2/\partial x^2 + \partial^2/\partial y^2 + \partial^2/\partial z^2 = \nabla_H^2 + \partial^2/\partial z^2$ is the three-dimensional Laplacian operator. This equation for the vertical velocity w can be used to derive the dispersion relation for internal gravity waves.

Internal Waves in a Stratified Fluid

The situation embodied in (7.134) is fundamentally different from that of interface waves because there is no obvious direction of propagation. For interface waves constrained to follow a horizontal surface with the x-axis chosen along the direction of wave propagation, a dispersion relation $\omega(k)$ was obtained that is independent of the wave direction. Furthermore, wave crests and wave groups propagate in the same direction, although at different speeds. However, in the current situation, the fluid is *continuously* stratified and internal waves might propagate in any direction and at any angle to the vertical. In such a case the *direction* of the wave number vector $\mathbf{K} = (k, l, m)$ becomes important and the dispersion relationship is *anisotropic* and depends on the wave number components:

$$\omega = \omega(k, l, m) = \omega(\mathbf{K}). \tag{7.135}$$

Consequently, the wave number, phase velocity, and group velocity are no longer scalars and the prototype sinusoidal wave (7.2) must be replaced with its three-dimensional extension (7.5). However, (7.135) must still be isotropic in k and l, the wave number components in the two horizontal directions.

The propagation of internal waves is a baroclinic process, in which the surfaces of constant pressure do not coincide with the surfaces of constant density. It was shown in Section 5.4, in connection with Kelvin's circulation theorem, that baroclinic processes generate vorticity. Internal waves in a continuously stratified fluid are therefore rotational. Waves at a density interface constitute a limiting case in which all the vorticity is concentrated in the form of a velocity discontinuity at the interface. The Laplace equation can therefore be used to describe the flow field within each layer. However, internal waves in a continuously stratified fluid cannot be described by the Laplace equation.

To reveal the structure of the situation described by (7.134) and (7.135), consider the complex version of (7.5) for the vertical velocity

$$w = w_0 e^{i(kx+ly+mz-\omega t)} = w_0 e^{i(\mathbf{K}\cdot\mathbf{x}-\omega t)} \tag{7.136}$$

in a fluid medium having a constant buoyancy frequency. Substituting (7.136) into (7.134) with constant N leads to the dispersion relation:

$$\omega^2 = \frac{k^2 + l^2}{k^2 + l^2 + m^2} N^2. \tag{7.137}$$

For simplicity choose the x-z plane so it contains $\mathbf{K}$ and $l = 0$. No generality is lost through this choice because the medium is horizontally isotropic, but k now represents the entire horizontal wave number and (7.137) can be written:

$$\omega = \frac{kN}{\sqrt{k^2 + m^2}} = \frac{kN}{K}. \tag{7.138}$$

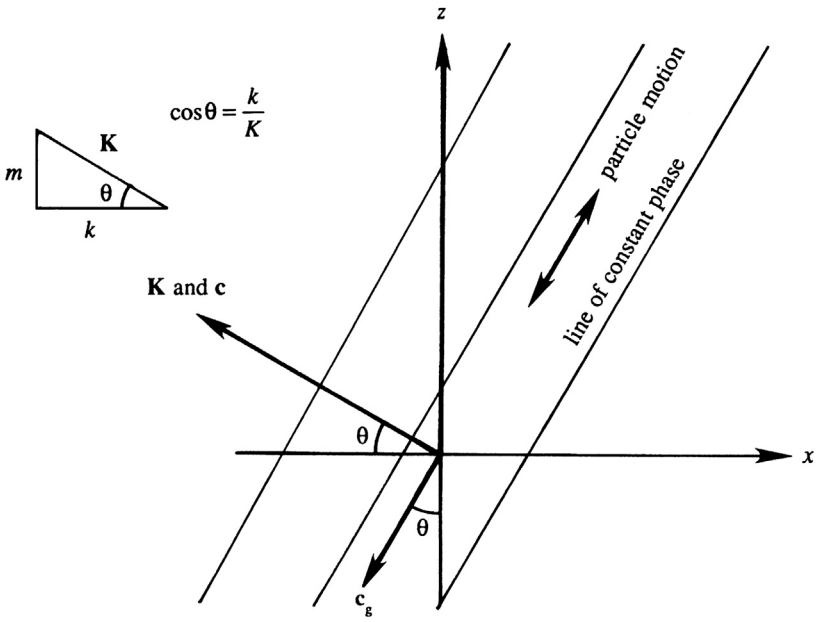

FIGURE 7.29 Geometric parameters for internal waves. Here z is vertical and x is horizontal. Note that $\mathbf{c}$ and $\mathbf{c}_g$ are at right angles and have opposite vertical components while $\mathbf{u}$ is parallel to the group velocity. Thus, internal wave packets slide along their crests.

This is the dispersion relation for internal gravity waves and can also be written as

$$\omega = N \cos \theta, \tag{7.139}$$

where $\theta = \tan^{-1}(m/k)$ is the angle between the phase velocity vector $\mathbf{c}$ (and therefore $\mathbf{K}$) and the horizontal direction (Figure 7.29). Interestingly, (7.139) states that the frequency of an internal wave in a stratified fluid depends only on the *direction* of the wave number vector and not on its magnitude. This is in sharp contrast with surface and interfacial gravity waves, for which frequency depends only on the magnitude. In addition, the wave frequency lies in the range $0 < \omega < N$, and this indicates that *N is the maximum possible frequency of internal waves in a stratified fluid*.

Before further investigation of the dispersion relation, consider particle motion in an incompressible internal wave. For consistency with (7.136), the horizontal fluid velocity is written as

$$u = u_0 \, e^{i(kx+ly+mz-\omega t)}, \tag{7.140}$$

plus two similar expressions for v and w. Differentiating produces:

$$\frac{\partial u}{\partial x} = iku_0 \, e^{i(kx+ly+mz-\omega t)} = iku.$$

Thus, (4.10) then requires that $ku + lv + mw = 0$, that is,

$$\mathbf{K} \cdot \mathbf{u} = 0, \tag{7.141}$$

showing that *particle motion is perpendicular to the wave number vector* (Figure 7.29). Note that only two conditions have been used to derive this result, namely the incompressible continuity equation and trigonometric behavior in *all* spatial directions. As such, the result is valid for many other wave systems that meet these two conditions. These waves are called *shear waves* (or transverse waves) because the fluid moves parallel to the constant phase lines. Surface or interfacial gravity waves do not have this property because the field varies *exponentially* in the vertical.

We can now interpret θ in the dispersion relation (7.139) as the angle between the particle motion and the *vertical* direction (Figure 7.29). The maximum frequency $\omega = N$ occurs when $\theta = 0$, that is, when the particles move up and down vertically. This case corresponds to $m = 0$ (see (7.138)), showing that the motion is independent of the z-coordinate. The resulting motion consists of a series of vertical columns, all oscillating at the buoyancy frequency N, with the flow field varying in the horizontal direction only.

At the opposite extreme we have $\omega = 0$ when $\theta = \pi/2$, that is, when the particle motion is completely horizontal. In this limit our internal wave solution (7.138) would seem to require $k = 0$, that is, horizontal independence of the motion. However, such a conclusion is not valid; pure horizontal motion is not a limiting case of internal waves, and it is necessary to examine the basic equations to draw any conclusion for this case. An examination of the governing set, (4.10) and (7.128) through (7.131), shows that a possible steady solution is $w = p' = \rho' = 0$, with u and v and *any* functions of x and y satisfying

$$\frac{\partial u}{\partial x} + \frac{\partial v}{\partial y} = 0. \tag{7.142}$$

The z-dependence of u and v is arbitrary. The motion is therefore two dimensional in the horizontal plane, with the motion in the various horizontal planes decoupled from each other. This is why clouds in the upper atmosphere seem to move in flat horizontal sheets, as often observed in airplane flights (Gill, 1982). For a similar reason a cloud pattern pierced by a mountain peak sometimes shows *Karman vortex streets*, a two-dimensional feature; see the striking photograph in Figure 9.19. A restriction of strong stratification is necessary for such almost horizontal flows, because (7.131) suggests that the vertical motion is small if N is large.

The foregoing discussion leads to the interesting phenomenon of *blocking* in a strongly stratified fluid. Consider a two-dimensional body placed in such a fluid, with its axis

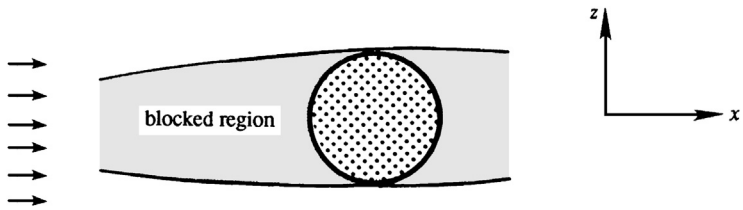

FIGURE 7.30 Blocking in strongly stratified flow. The circular region represents a two-dimensional body with its axis along the y direction (perpendicular to the page). Horizontal flow in the shaded region is blocked by the body when the stratification is strong enough to prevent fluid in the blocked layer from going over or under the body.

horizontal (Figure 7.30). The two dimensionality of the body requires $\partial v/\partial y = 0$, so that the continuity equation (7.142) reduces to $\partial u/\partial x = 0$. A horizontal layer of fluid ahead of the body, bounded by tangents above and below it, is therefore blocked and held motionless. (For photographic evidence see Figure 3.18 in the book by Turner (1973).) This happens because the strong stratification suppresses the w field and prevents the fluid from going below or over the body.

Dispersion of Internal Waves in a Stratified Fluid

The dispersion relationship (7.138) for linear internal waves with constant buoyancy frequency contains a few genuine surprises that challenge our imaginations and violate the intuition acquired by observing surface or interface waves. One of these surprises involves the phase, $\mathbf{c}$, and group, $\mathbf{c}_g$, velocity vectors. In multiple dimensions, these are defined by

$$\mathbf{c} = (\omega/K)\mathbf{e}_K \quad \text{and} \quad \mathbf{c}_g = \mathbf{e}_x\frac{\partial\omega}{\partial k} + \mathbf{e}_y\frac{\partial\omega}{\partial l} + \mathbf{e}_z\frac{\partial\omega}{\partial m}, \tag{7.8, 7.143}$$

where $\mathbf{e}_K = \mathbf{K}/K$. Interface waves $\mathbf{c}$ and $\mathbf{c}_g$ are in the same direction, although their magnitudes can be different. For internal waves, (7.138), (7.8), and (7.143) can be used to determine:

$$\mathbf{c} = \frac{\omega}{K^2}(k\mathbf{e}_x + m\mathbf{e}_z), \quad \text{and} \quad \mathbf{c}_g = \frac{Nm}{K^3}(m\mathbf{e}_x - k\mathbf{e}_z). \tag{7.144, 7.145}$$

Forming the dot product of these two equations produces:

$$\mathbf{c}_g \cdot \mathbf{c} = 0! \tag{7.146}$$

Thus, the *phase and group velocity vectors are perpendicular* as shown on Figure 7.29. Equations (7.144) and (7.145) do place the horizontal components of $\mathbf{c}$ and $\mathbf{c}_g$ in the same direction, but their vertical components are equal and opposite. In fact, $\mathbf{c}$ and $\mathbf{c}_g$ form two sides of a right triangle whose hypotenuse is horizontal (Figure 7.31). Consequently, the phase velocity has an upward component when the group velocity has a downward component, and vice versa. Equations (7.141) and (7.146) are consistent because $\mathbf{c}$ and $\mathbf{K}$ are parallel and $\mathbf{c}_g$ and $\mathbf{u}$ are

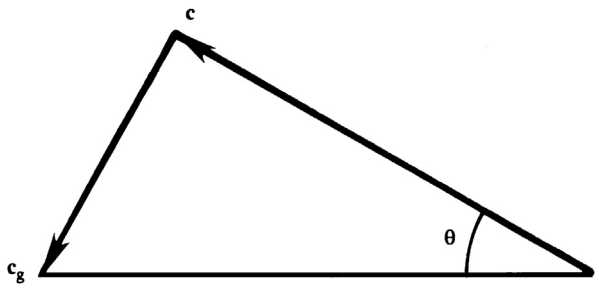

FIGURE 7.31 Orientation of phase and group velocity for internal waves. The vertical components of the phase and group velocities are equal and opposite.

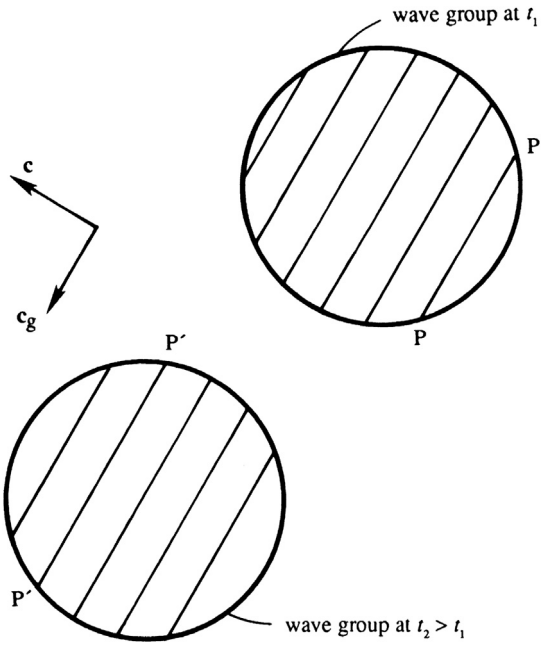

FIGURE 7.32 Illustration of phase and group propagation in a circular internal-wave packet. Positions of the wave packet at two times are shown. The constant-phase line PP (a crest perhaps) at time t_1 propagates to P′P′ at t_2.

parallel. The fact that **c** and $\mathbf{c}_g$ are perpendicular, and have opposite vertical components, is illustrated in Figure 7.32. It shows that the phase lines are propagating toward the left and upward, whereas the wave group is propagating to the left and downward. Wave crests are constantly appearing at one edge of the group, propagating through the group, and vanishing at the other edge.

The group velocity here has the usual significance of being the velocity of propagation of energy of a certain sinusoidal component. Suppose a source is oscillating at frequency ω. Then its energy will only be transmitted outward along four beams oriented at an angle θ with the vertical, where $\cos\theta = \omega/N$. This has been verified in a laboratory experiment (Figure 7.33). The source in this case was a vertically oscillating cylinder with its axis perpendicular to the plane of paper. The frequency was $\omega < N$. The light and dark lines in the photograph are lines of constant density, made visible by an optical technique. The experiment showed that the energy radiated along four beams that became more vertical as the frequency was increased, which agrees with $\cos\theta = \omega/N$.

These results were obtained by assuming that N is depth independent, an assumption that may seem unrealistic at first. Figure 13.2 shows N vs. depth for the deep ocean, and $N < 0.01$ rad./s everywhere, but N is largest between ~200 m and ~2 km. These results can be considered *locally* valid if N varies slowly over the vertical wavelength $2\pi/m$ of the motion. The so-called *WKB approximation* for internal waves, in which such a slow variation of $N(z)$ is not neglected, is discussed in Chapter 13.

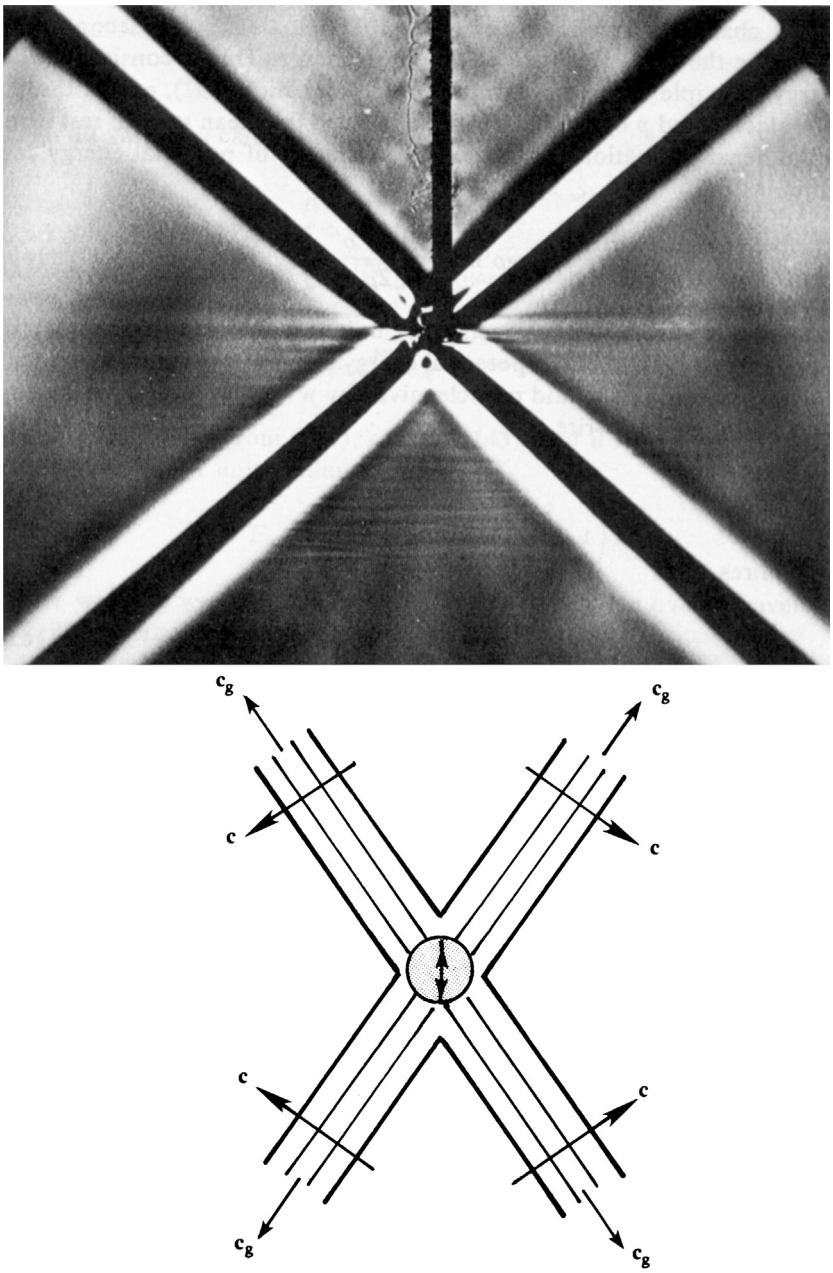

FIGURE 7.33 Waves generated in a stratified fluid of uniform buoyancy frequency $N = 1$ rad./s. The forcing agency is a horizontal cylinder, with its axis perpendicular to the plane of the paper, oscillating vertically at frequency $\omega = 0.71$ rad./s. With $\omega/N = 0.71 = \cos\theta$, this agrees with the observed angle of $\theta = 45°$ made by the beams with the horizontal direction. The vertical dark line in the upper half of the photograph is the cylinder support and should be ignored. The light and dark radial lines represent contours of constant ρ' and are therefore constant phase lines. The schematic diagram below the photograph shows the directions of $\mathbf{c}$ and $\mathbf{c}_g$ for the four beams. *Reprinted with the permission of Dr. T. Neil Stevenson, University of Manchester.*

Energy Considerations for Internal Waves in a Stratified Fluid

The energy carried by an internal wave travels in the direction and at the speed of the group velocity. To show this is the case, construct a mechanical energy equation from (7.128) through (7.130) by multiplying the first equation by $\rho_0 u$, the second by $\rho_0 v$, the third by $\rho_0 w$, and summing the results to find:

$$\frac{\partial}{\partial t}\left[\frac{1}{2}\rho_0(u^2+v^2+w^2)\right] + g\rho' w + \nabla\cdot(p'\mathbf{u}) = 0. \tag{7.147}$$

Here the continuity equation has been used to write $u(\partial p'/\partial x) + v(\partial p'/\partial y) + w(\partial p'/\partial z) = \nabla \cdot (p'\mathbf{u})$, which represents the net work done by pressure forces. Another interpretation is that $\nabla\cdot(p'\mathbf{u})$ is the divergence of the *energy flux* $p'\mathbf{u}$, which must change the wave energy at a point. As the first term in (7.147) is the rate of change of kinetic energy, we can anticipate that the second term $g\rho' w$ must be the rate of change of potential energy. This is consistent with the energy principle derived in Chapter 4 (see (4.56)), except that ρ' and p' replace ρ and p because we have subtracted the mean state of rest here. Using the density equation (7.131), the rate of change of potential energy can be written as

$$\frac{\partial E_{\mathrm{P}}}{\partial t} = g\rho' w = \frac{\partial}{\partial t}\left[\frac{g^2\rho'^2}{2\rho_0 N^2}\right], \tag{7.148}$$

which shows that the potential energy per unit volume must be the positive quantity $Ep = \mathrm{g}^2\rho'^2/2\rho_0 N^2$. The potential energy can also be expressed in terms of the displacement ζ of a fluid particle, given by $w = \partial\zeta/\partial t$. Using the density equation (7.131), we can write

$$\frac{\partial \rho\prime}{\partial t} = \frac{N^2\rho_0}{g}\frac{\partial \zeta}{\partial t}, \quad \text{which requires that } \rho' = \frac{N^2\rho_0\zeta}{g}. \tag{7.149}$$

The potential energy *per unit volume* is therefore

$$E_{\mathrm{P}} = \frac{g^2\rho'^2}{2\rho_0 N^2} = \frac{1}{2}N^2\rho_0\zeta^2. \tag{7.150}$$

This expression is consistent with our previous result from (7.96) for two infinitely deep fluids, for which the average potential energy of the entire water column *per unit horizontal area* was shown to be

$$\frac{1}{4}(\rho_2-\rho_1)ga^2, \tag{7.151}$$

where the interface displacement is of the form $\zeta = a\cos(kx-\omega t)$ and $(\rho_2-\rho_1)$ is the density discontinuity. To see the consistency, we shall symbolically represent the buoyancy frequency of a density discontinuity at $z=0$ as

$$N^2 = -\frac{g}{\rho_0}\frac{d\overline{\rho}}{dz} = \frac{g}{\rho_0}(\rho_2-\rho_1)\delta(z), \tag{7.152}$$

where $\delta(z)$ is the Dirac delta function (see Appendix B.4). (As with other relations involving the delta function, equation (7.152) is valid in the *integral* sense, that is, the integral (across the

origin) of the last two terms is equal because $\int \delta(z)\, dz = 1$.) Using (7.152), a vertical integral of (7.150), coupled with horizontal averaging over a wavelength, gives the expression (7.151). Note that for surface or interfacial waves, E_k and E_p represent kinetic and potential energies of the entire water column, per unit horizontal area. In a continuously stratified fluid, they represent energies per unit volume.

We shall now demonstrate that the average kinetic and potential energies are equal for internal wave motion. Assume periodic solutions

$$\left[u, w, p', \rho'\right] = \left[\widehat{u}, \widehat{w}, \widehat{p}, \widehat{\rho}\right]\, e^{i(kx+mz-\omega t)}.$$

Then all variables can be expressed in terms of w:

$$p' = -\frac{\omega m \rho_0}{k^2}\widehat{w}\; e^{i(kx+mz-\omega t)}, \rho' = \frac{iN^2\rho_0}{\omega g}\widehat{w}\; e^{i(kx+mz-\omega t)}, u = -\frac{m}{k}\widehat{w}\; e^{i(kx+mz-\omega t)}, \tag{7.153}$$

where p' is derived from (7.132), ρ' from (7.131), and u from (7.128). The average kinetic energy per unit volume is therefore

$$E_\mathrm{k} = \frac{1}{2}\rho_0\overline{(u^2+w^2)} = \frac{1}{4}\rho_0\left(\frac{m^2}{k^2}+1\right)\widehat{w}^2, \tag{7.154}$$

where we have taken real parts of the various expressions in (7.153) before computing quadratic quantities and used the fact that the average of $\cos^2()$ over a wavelength is ½. The average potential energy per unit volume is

$$E_\mathrm{p} = \frac{g^2\overline{\rho'^2}}{2\rho_0 N^2} = \frac{N^2\rho_0}{4\omega^2}\widehat{w}^2, \tag{7.155}$$

where we have used $\overline{\rho'^2} = \widehat{w}^2N^4\rho_0^2/2\omega^2g^2$, found from (7.153) after taking its real part. Use of the dispersion relation $\omega^2 = k^2N^2/(k^2+m^2)$ shows that

$$E_\mathrm{k} = E_\mathrm{p}, \tag{7.156}$$

which is a general result for small oscillations of a conservative system without Coriolis forces. The total wave energy is

$$E = E_\mathrm{k} + E_\mathrm{p} = \frac{1}{2}\rho_0\left(\frac{m^2}{k^2}+1\right)\widehat{w}^2. \tag{7.157}$$

Last, we shall show that $\mathbf{c}_\mathrm{g}$ times the wave energy equals the energy flux. The average energy flux $\mathbf{F}$ across a unit area can be found from (7.153):

$$\mathbf{F} = \overline{p'\mathbf{u}} = \mathbf{e}_x\overline{p'u} + \mathbf{e}_z\overline{p'w} = \frac{\rho_0\omega m\widehat{w}^2}{2k^2}\left(\mathbf{e}_x\frac{m}{k} - \mathbf{e}_z\right). \tag{7.158}$$

Using (7.145) and (7.157), group velocity times wave energy is

$$\mathbf{c}_\mathrm{g}E = \frac{Nm}{K^3}(m\mathbf{e}_x - k\mathbf{e}_z)\left[\frac{\rho_0}{2}\left(\frac{m^2}{k^2}+1\right)\widehat{w}^2\right],$$

which reduces to (7.158) on using the dispersion relation (7.138), so it follows that

$$\mathbf{F} = \mathbf{c}_g E. \tag{7.159}$$

This result also holds for surface or interfacial gravity waves. However, in that case **F** represents the flux per unit width perpendicular to the propagation direction (integrated over the entire depth), and E represents the energy per unit horizontal area. In (7.159), on the other hand, **F** is the flux per unit area, and E is the energy per unit volume.

EXERCISES

7.1. Starting from (7.5) and working in (x, y, z) Cartesian coordinates, determine an equation that specifies the locus of points that defines a wave crest. Verify that the travel speed of the crests in the direction of $\mathbf{K} = (k, l, m)$ is $c = \omega/|\mathbf{K}|$. Can anything be determined about the wave crest travel speed in other directions?

7.2. For $ka \ll 1$, use the potential for linear deep-water waves $\phi(z,x,t) = a(\omega/k)e^{kz}\sin(kx - \omega t)$ and the waveform $\eta(x,t) = a\cos(kx - \omega t) + \alpha k a^2 \cos[2(kx - \omega t)]$ to show that:

a) With an appropriate choice of the constant α, the kinematic boundary condition (7.16) can be satisfied for terms proportional to $(ka)^0$ and $(ka)^1$ once the common factor of $a\omega$ has been divided out.

b) With an appropriate choice of the constant γ, the dynamic boundary condition (7.19) can be satisfied for terms proportional to $(ka)^0$, $(ka)^1$, and $(ka)^2$ when $\omega^2 = gk(1 + \gamma k^2 a^2)$ once the common factor of ag has been divided out.

7.3. The field equation for surface waves on a deep fluid layer in two dimensions (x,z) is: $\dfrac{\partial^2\phi}{\partial x^2} + \dfrac{\partial^2\phi}{\partial z^2} = 0$, where ϕ is the velocity potential, $\nabla\phi = (u, w)$. The linearized free-surface boundary conditions and the bottom boundary condition are:

$$(\partial\phi/\partial z)_{z=0} \cong \partial\eta/\partial t,\ (\partial\phi/\partial t)_{z=0} + g\eta \cong 0, \text{ and } (\partial\phi/\partial z)_{z\to-\infty} = 0,$$

where $z = \eta(x,t)$ defines the free surface, gravity g points downward along the z-axis, and the undisturbed free surface lies at $z = 0$. The goal of this problem is to develop the general solution for these equations without assuming a sinusoidal form for the free surface as was done in Sections 7.1 and 7.2.

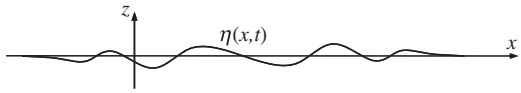

a) Assume $\phi(x,z,t) = \Lambda(x,t)Z(z)$, and use the field equation and bottom boundary condition to show that $\phi(x,z,t) = \Lambda(x,t)\exp(+kz)$, where k is a positive real constant.

b) Use the results of part a) and the remaining boundary conditions to show:

$$\frac{\partial^2\Lambda}{\partial t^2} + gk\Lambda = 0 \quad \text{and} \quad \frac{\partial^2\Lambda}{\partial x^2} + k^2\Lambda = 0.$$

c) For a fixed value of k, find $\Lambda(x, t)$ in terms of four unknown amplitudes A, B, C, and D.
d) For the initial conditions: $\eta = h(x)$ and $\partial\eta/\partial t = \dot{h}(x)$ at $t = 0$, determine the general form of $\phi(x, z, t)$.

7.4. Derive (7.37) from (7.27).

7.5. Consider stationary surface gravity waves in a rectangular container of length L and breadth b, containing water of undisturbed depth H. Show that the velocity potential $\phi = A\cos(m\pi x/L)\cos(n\pi y/b)\cosh k(z+H)\, e^{-i\omega t}$ satisfies the Laplace equation and the wall boundary conditions, if $(m\pi/L)^2+(n\pi/b)^2 = k^2$. Here m and n are integers. To satisfy the linearized free-surface boundary condition, show that the allowable frequencies must be $\omega^2 = gk\tanh kH$. [*Hint*: combine the two boundary conditions (7.18) and (7.21) into a single equation $\partial^2\phi/\partial t^2 = -g\,\partial\phi/\partial z$ at $z = 0$.]

7.6. A lake has the following dimensions: $L = 30$ km, $b = 2$ km, and $H = 100$ m. If the wind sets up the mode $m = 1$ and $n = 0$, show that the period of the oscillation is 31.7 min.

7.7. Fill a square or rectangular cake pan half way with water. Do the same for a round frying pan of about the same size. Agitate the water by carrying the two pans while walking briskly (outside) at a consistent pace on a horizontal surface.
a) Which shape lends itself better to spilling?
b) At what portion of the perimeter of the rectangular pan does spilling occur most readily?
c) Explain your observations in terms of standing wave modes.

7.8. Using the approach of (7.43), show that the time-average energy flux F per unit length of crest is zero for the standing wave described by (7.62).

7.9. Show that the group velocity of pure capillary waves in deep water, for which the gravitational effects are negligible, is $c_g = \dfrac{3}{2}c$.

7.10. Plot the group velocity of surface gravity waves, including surface tension σ, as a function of λ.
a) Assuming deep water, show that the group velocity is

$$c_g = \frac{1}{2}\sqrt{\frac{g}{k}}\frac{1+3\sigma k^2/\rho g}{\sqrt{1+\sigma k^2/\rho g}}.$$

b) Show that this becomes minimum at a wave number given by

$$\frac{\sigma k^2}{\rho g} = \frac{2}{\sqrt{3}} - 1.$$

c) For cool water ($\rho = 1000$ kg/m^3 and $\sigma = 0.074$ N/m), verify that $c_{g\,\min} = 17.8$ cm/s.

7.11. The effect of viscosity on the energy of linear deep-water surface waves can be determined from the wave motion's velocity components and the viscous dissipation (4.58).
a) For incompressible flow, the viscous dissipation of energy per unit mass of fluid is $\varepsilon = 2(\mu/\rho)S_{ij}^2$, where S_{ij} is the strain-rate tensor and μ is the fluid's viscosity. Determine ε using (7.47).
b) The total wave energy per unit surface area, E, for a linear sinusoidal water wave with amplitude a is given by (7.42). Assume that a is a function of time, set $dE/dt = -\varepsilon$, and show that $a(t) = a_0\exp[-2(\mu/\rho)k^2 t]$, where a_0 is the wave amplitude at $t = 0$.

c) Using a nominal value of $\mu/\rho = 10^{-6}$ m^2/s for water, determine the time necessary for an amplitude reduction of 50% for water-surface waves having $\lambda = 1$ mm, 1 cm, 10 cm, 1 m, 10 m, and 100 m.

d) Convert the times calculated in part c) to travel distances by multiplication with an appropriate group speed. Remember to include surface tension. Can a typhoon located near New Zealand produce increased surf on the west coast of North America? [The circumference of the earth is approximately 40,000 km.]

7.12. Consider a deep-water wave train with a Gaussian envelope that resides near $x = 0$ at $t = 0$ and travels in the positive x direction. The surface shape at any time is a Fourier superposition of waves with all possible wave numbers:

$$\eta(x,t) = \int_{-\infty}^{+\infty} \tilde{\eta}(k)\exp\Big[i\Big(kx - (g|k|)^{1/2}t\Big)\Big]dk, \qquad (\dagger)$$

where $\tilde{\eta}(k)$ is the amplitude of the wave component with wave number k, and the dispersion relation is $\omega = (gk)^{1/2}$. For the following items assume the surface shape at $t = 0$ is:

$$\eta(x,0) = \frac{1}{\sqrt{2\pi}\alpha}\ \exp\left\{-\frac{x^2}{2\alpha^2} + ik_d x\right\}.$$

Here, $k_d > 0$ is the dominant wave number, and α sets the initial horizontal extent of the wave train, with larger α producing a longer wave train.

a) Plot Re$\{\eta(x, 0)\}$ for $|x| \le 40\ m$ when $\alpha = 10\ m$ and $k_d = 2\pi/\lambda_d = 2\pi/10\ m^{-1}$.

b) Use the inverse Fourier transform at $t = 0$, $\tilde{\eta}(k) = (1/2\pi)\int_{-\infty}^{+\infty} \eta(x,0)\exp[-ikx]dx$ to find the wave amplitude distribution: $\tilde{\eta}(k) = (1/2\pi)\exp\left\{-\frac{1}{2}(k - k_d)^2\alpha^2\right\}$, and plot this function for $0 < k < 2k_d$ using the numerical values from part a). Does the dominant contribution to the wave activity come from wave numbers near k_d for the part a) values?

c) For large x and t, the integrand of (†) will be highly oscillatory unless the phase $\Phi \equiv kx - (g|k|)^{1/2}t$ happens to be constant. Thus, for any x and t, the primary contribution to η will come from the region where the phase in (†) does not depend on k. Thus, set $d\Phi/dk = 0$, and solve for k_s (= the wave number where the phase is independent of k) in terms of x, t, and g.

d) Based on the result of part b), set $k_s = k_d$ to find the x-location where the dominant portion of the wave activity occurs at time t. At this location, the ratio x/t is the propagation speed of the dominant portion of the wave activity. Is this propagation speed the phase speed, the group speed, or another speed altogether?

7.13. Show that the vertical component of the Stokes drift is zero starting from (7.85) and using (7.47) and (7.48).

7.14. Extend the deep water Stokes drift result (7.85) to arbitrary depth to derive (7.86).

7.15. Explicitly show through substitution and differentiation that (7.88) is a solution of (7.87).

7.16. A *thermocline* is a thin layer in the upper ocean across which water temperature and, consequently, water density change rapidly. Suppose the thermocline in a very deep ocean is at a depth of 100 m from the ocean surface, and that the temperature drops

across it from 30°C to 20°C. Show that the reduced gravity is $g' = 0.025$ m/s^2. Neglecting Coriolis effects, show that the speed of propagation of long gravity waves on such a thermocline is 1.58 m/s.

7.17. Consider internal waves in a continuously stratified fluid of buoyancy frequency $N = 0.02$ s^{-1} and average density 800 kg/m^3. What is the direction of ray paths if the frequency of oscillation is $\omega = 0.01$ s^{-1}? Find the energy flux per unit area if the amplitude of the vertical velocity is $\widehat{w} = 1$ cm/s and the horizontal wavelength is π meters.

7.18. Consider internal waves at a density interface between two infinitely deep fluids, and show that the average kinetic energy per unit horizontal area is $E_k = (\rho_2 - \rho_1)ga^2/4$.

7.19. Consider waves in a finite layer overlying an infinitely deep fluid. Using the constants given in equations (7.106) through (7.109), prove the dispersion relation (7.110).

7.20. A simple model of oceanic internal waves involves two ideal incompressible fluids ($\rho_2 > \rho_1$) trapped between two horizontal surfaces at $z = h_1$ and $z = -h_2$, and having an average interface location of $z = 0$. For traveling waves on the interface, assume that the interface deflection from $z = 0$ is $\xi = \xi_o \,\mathrm{Re}\{\exp(i(\omega t - kx))\}$. The phase speed of the waves is $c = \omega/k$.

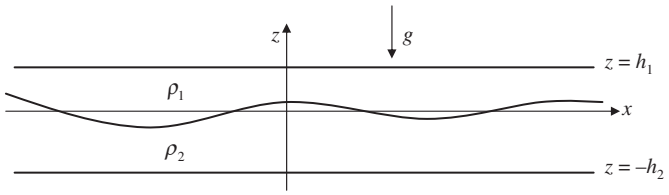

a) Show that the dispersion relationship is $\omega^2 = \dfrac{gk(\rho_2 - \rho_1)}{\rho_2 \coth(kh_2) + \rho_1 \coth(kh_1)}$, where g is the acceleration of gravity.

b) Determine the limiting form of c for short (i.e., unconfined) waves, kh_1 and $kh_2 \to \infty$.

c) Determine the limiting form of c for long (i.e., confined) waves, kh_1 and $kh_2 \to 0$.

d) At fixed wavelength λ (or fixed $k = 2\pi/\lambda$), do confined waves go faster or slower than unconfined waves?

e) At a fixed frequency, what happens to the wavelength and phase speed as $\rho_2 - \rho_1 \to 0$?

f) What happens if $\rho_2 < \rho_1$?

Literature Cited

Gill, A. (1982). *Atmosphere–Ocean Dynamics*. New York: Academic Press.
Graff, K. A. (1975). *Wave Motion in Elastic Solids*. Oxford: Oxford University Press.
Kinsman, B. (1965). *Wind Waves*. Englewood Cliffs, New Jersey: Prentice-Hall.
LeBlond, P. H., & Mysak, L. A. (1978). *Waves in the Ocean*. Amsterdam: Elsevier Scientific Publishing.
Liepmann, H. W., & Roshko, A. (1957). *Elements of Gasdynamics*. New York: Wiley.
Lighthill, M. J. (1978). *Waves in Fluids*. London: Cambridge University Press.
Phillips, O. M. (1977). *The Dynamics of the Upper Ocean*. London: Cambridge University Press.
Turner, J. S. (1973). *Buoyancy Effects in Fluids*. London: Cambridge University Press.
Whitham, G. B. (1974). *Linear and Nonlinear Waves*. New York: Wiley.